Performance Analysis of Attitude Determination Algorithms for Low Cost Attitude Heading Reference Systems

by

Karthik Narayanan

A dissertation submitted to the Graduate Faculty of
Auburn University
in partial fulfillment of the
requirements for the Degree of
Doctor of Philosophy

Auburn, Alabama
August 9, 2010

Keywords: attitude estimation, quaternion, nonlinear observer

Approved by:

Michael E. Greene, Chair, Professor Emeritus of Electrical and Computer Engineering
Thomas Denney, Associate Professor of Electrical and Computer Engineering
John E. Cochran, Jr., Professor and Head of Aerospace Engineering

Abstract

Development of micro-electro mechanical system (MEMS) and micro-electro optical mechanical system (MEOMS) inertial sensors has been driven by the need for inexpensive sensing solutions in military and commercial applications. In addition to traditional attitude estimation and automobile applications, the reduced cost of MEMS/MEOMS inertial sensors has spurred new applications in personal navigation, pose estimation, audio visualization, cueing, etc. Electromechanical inertial sensors are also increasingly used in low cost attitude heading reference systems (AHRS) and backup attitude indicators, when the required accuracies are not too stringent. With the current performance levels of MEMS sensors, AHRS systems using electromechanical sensors rely on some form of external aiding to generate a better attitude solution. External aiding could come from an air data computer, global positioning system (GPS), etc., but the aiding comes at an increased cost. Aiding sources have their own set of errors and may not be available at all times. For example, air data sources suffer from problems such as icing, blocked pressure ports etc., and GPS integrity can be compromised due to interference. This dissertation addresses the problem of low cost attitude estimation using a triad of MEMS gyros and accelerometers for fixed wing and rotary wing aircrafts, under conditions when external aiding is unavailable or not useful. Using angular rate, acceleration and magnetic measures, a unit quaternion algorithm is formulated by combining a non linear attitude estimator with fuzzy logic concepts. Static and dynamic conditions of the aircraft are exploited to adaptively alter gains in correction loops used to correct input rate measures. Standard tests are simulated to assess the performance of the formulated algorithm. Real world flight data is used to compare the results of the proposed algorithm with an extended Kalman filter, and the error analysis is presented. It is shown that the fuzzy non linear estimator algorithm can be used to compute a reasonably accurate attitude solution using inexpensive MEMS sensors, even when external sources of aiding are unavailable.

Acknowledgments

I would like to thank my advisor Dr. Michael Greene for his guidance through this long effort. Without his periodic reminders and and encouragement this dissertation would not have been possible. Dr. Greene's breadth of knowledge in many areas has been a continued source of inspiration to me. I would like to thank the advisory committee members Dr. Denney, Dr. Cochran, and Dr. Sinclair for their suggestions to improve this dissertation. Special thanks are due to Mr. Victor Trent, my supervisor at Archangel Systems, for his enormous encouragement and help. I am very thankful to Archangel Systems for letting me use measurement sensors and flight test data. I am indebted to my closest of friends who have helped me through some tough times. Finally, I thank my family for their support during my graduate studies.

Table of Contents

List of Figures

Chapter 1

Introduction

1.1 Overview

Attitude and Heading Reference Systems are used as a part of electronic flight information systems to provide aircraft pitch, roll and heading angles. In addition to delta angles and delta velocities provided by inertial measurement units, AHRS provide estimates of platform attitude. These inertial sensing systems use a triad of gyroscopes, accelerometers and a magnetometer to measure angular rates, linear accelerations and the earth's magnetic field. Target applications have traditionally been in navigation, guidance and control to provide body rates, accelerations and attitude to flight control systems (FCS), primary flight displays (PFD) and autopilot systems. Until recently, technologies like ring laser (RLG) and fiber optic gyros (FOG) have been the preferred choices given their performance and reliability. The associated costs of these sensor systems coupled with restrictions on exporting the enabling technologies have led to the rapid development of micro-eletromechanical (MEMS) technology aimed at reducing unit size and cost. MEMS sensors are usually classified as automotive-grade - as opposed to navigation grade, due to the difference in their performance. For example, as illustrated in Figure 1.1[6], current automotive grade MEMS gyroscopes have bias drifts of the order of 50-100 deg/hour, compared to 0.01 deg/hour with a navigation-grade gyro.

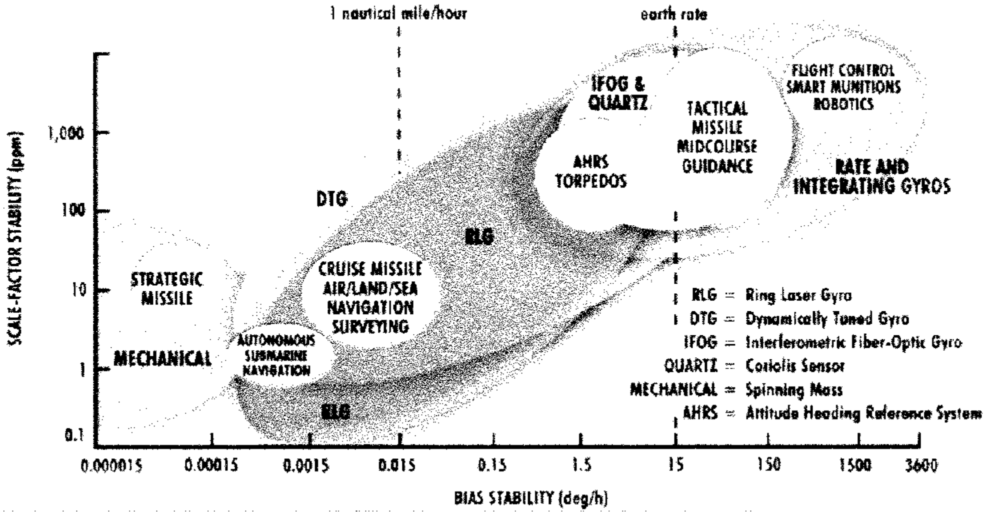

Figure 1.1: Inertial Sensors Comparison

In applications such as navigation and attitude estimation, the accuracy of the outputs is a direct function of the quality of sensing. Although the output estimates can degrade with time, non-jammability, high data rates, and bandwidth are some of the attractive features of inertial navigation systems (INS), AHRS, and inertial measurement systems (IMU).

1.2 The Case for MEMS Inertial Sensing

Although the reduced accuracy of MEMS sensors is a drawback, the usage of these inexpensive sensors has only been gaining in popularity, mainly due to the relatively high cost of inertial sensing with traditional mechanical sensors. A number of reasons are attributed to the recent growth of silicon and quartz-based inertial sensors - understanding of the sensing elements, their interaction with the support electronics, plan wall etching and significant investment to develop a single-chip solution[9]. Given the high volume of production, automotive applications such as crash protection, roll over sensing etc. have further spurred the move toward lower cost per sense axis. Some of the advantages of the MEMS sensors are

- Smaller footprint.

- Lower weight and power consumption.
- Higher volume of production at a lower cost.
- Lower part counts resulting in lower maintenance.

While navigation applications still require accuracies not currently met by MEMS sensors, other areas such as AHRS, personal navigation, crash testing, graphics, etc. have helped sustain the growth. A major factor that has contributed to the penetration of MEMS sensors is the idea of external aiding. Aiding sources like air data systems, Doppler sensors, global positioning system (GPS) signals etc. help alleviate the reduced acuracy of the MEMS sensors, by providing independent measures. While an improvement in position and velocity accuracy is a direct result of external aiding, attitude estimates in an AHRS, for example, also improve. Aiding sources, not surprisingly, are far from perfect and suffer from problems such as low update rates, jammability, interference etc. For example, GPS signals suffer from interference and the obtained velocity estimates are noisy at low speeds. Air data from static and pitot sources suffer from installation specific errors that are difficult to model. Processing algorithms have been devised to account for aiding errors, but this in turn increases the development cost of the system. In applications such as hover on point, aiding sources such as GPS do not provide adequate information. Given the costs and problems associated with aiding, fixed-wing and rotary wing aircrafts in the general aviation market require reasonable attitude accuracies, in the event of a loss or absence of aiding. With redundant systems, for example two or three AHRS, per aircraft, the cost of attitude sensing becomes more important.

1.3 Thesis Contributions and Organization

The focus of this dissertation is on the development of an attitude estimation algorithm using low cost MEMS sensors for an AHRS application. Emphasis is placed on using the minimum sensing package needed to achieve an acceptable accuracy. The performance of the attitude estimation algorithm with aiding is compared with other estimators to verify baseline performance. The achievable accuracy, under loss of aiding, is determined through flight test studies and compared with an Euler angle estimation algorithm with no aiding. The following are the contributions of this dissertation:

- Development of an algorithm that can provide reasonable attitude estimates without aiding when required.
- Use of sensor models to design the proposed algorithm.
- Comparison of algorithm results with those achieved using a traditional Kalman filter.
- Evaluation of the algorithm with simulated and real world sensor data.

To meet these objectives, this dissertation is organized as follows. Chapter 2 details the attitude representations and explores previous work in attitude estimation. Chapter 3 details the sensor models and calibration techniques for the MEMS sensors. Sensor model parameters are determined from experimental data to understand the performance limitations and determine the the extent of augmentation necessary. For example, information from Allan Variance plots of a MEMS gyro is used as an aid in choosing correction gains to reduce attitude error growth. Chapter 4 covers the development of the attitude estimation algorithm based on the quaternion formulation of a complementary filter in the special orthogonal group. Chapter 5 presents the results of tests with simulated and real world data, and compares them to those obtained using a Kalman filter attitude estimator with air data aiding. Chapter 6 provides conclusions and presents some ideas for future work.

Chapter 2

Attitude Estimation and Fuzzy Logic

2.1 Overview

Attitude estimation has received considerable attention in the literature. Traditional AHRS used gimballed mechanical gyros that remained to sense attitude with respect to an inertial frame. Modern strapdown systems measure angular rates and linear accelerations of a body-fixed frame with respect to a non rotating inertial frame and demand higher dynamic ranges from the sensors. The measurements of angular rates and specific forces are coordinatized in a body fixed frame. This chapter presents some of the representations of platform attitude, along with their advantages and drawbacks, and surveys the attitude estimation techniques in literature. An overview of classical complementary filtering in the s-domain is also presented, followed by a review of work on SO(3) complementary filtering. A review of fuzzy logic concepts is given to conclude the chapter.

2.2 Attitude Representations

The attitude estimation problem is formulated using two reference frames - a non-rotating (inertial) frame and a rotating (body-fixed) frame and . Let A and B represent the inertial reference frame and the rotating frame respectively. Depending on the set chosen, the orientation of B with respect to A can be represented using several different sets of parameters. In the following sections and chapters, the frame aligned with the magnetic north and the local vertical is taken to be the inertial frame and the rotating frame is fixed to the body of the aircraft as shown in Figure 2.1.

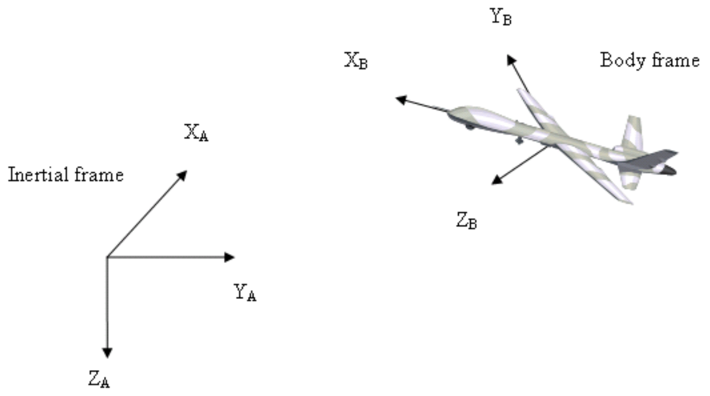

Figure 2.1: Coordinates Frames

The axes X_A, Y_A and Z_A of the inertial frame are assumed to be aligned with the north, east and down directions. X_B, Y_B and Z_B are defined to be the longitudinal, lateral and normal body axes. Roll, pitch and yaw motions are defined as a set of Euler angles as described in the following subsection.

2.2.1 Euler Angles

Euler angle representations of platform attitude are the simplest and easy to visualize. In this representation, the orientation of B with respect to A is represented by a sequence of three rotations from the reference frame to the rotating frame. If the three dextral, orthogonal axes of the inertial frame are named X_A, Y_A and Z_A, then successive rotations about three distinct axes can be used to specify the orientation of the rotating frame axes X_B, Y_B and Z_B. Although there are twelve possible choices of rotation sequences, the sequence 3-2-1 (starting with the Z_A axis) is widely used. The three rotation angles are usually termed roll, pitch and yaw angles. If ϕ, θ and ψ represent the roll, pitch and yaw Euler angles respectively, then the relationships between the time rates of change of the Euler angles and the components of angular velocity are given by

$$\begin{bmatrix} \dot{\phi} \\ \dot{\theta} \\ \dot{\psi} \end{bmatrix} = \begin{bmatrix} 1 & \sin\phi\tan\theta & \cos\phi\tan\theta \\ 0 & \cos\phi & -\sin\phi \\ 0 & \dfrac{\sin\phi}{\cos\theta} & \dfrac{\cos\phi}{\cos\theta} \end{bmatrix} \begin{bmatrix} \omega_x \\ \omega_y \\ \omega_z \end{bmatrix} \tag{2.1}$$

Here ω_x, ω_y and ω_z are the x, y and z-axis components of the body frame angular velocities. The Euler angles can be obtained by integrating the above equations. It is important to note that $\dot{\phi}$, $\dot{\theta}$ and $\dot{\psi}$ represent the angular rates of intermediate frames and do not form a vector. Euler angles are conceptually easy to visualize but suffer from singularity at $\theta = \frac{n\pi}{2}, n = \pm1, \pm3, \pm5$ etc., for the 3-2-1 rotation sequence. The attitude propagation equations for each choice of rotation sequence contain a similar singularity.

2.2.2 Direction Cosine Matrix

Another representation of relative orientation between two coordinate frames is the direction cosine matrix. A vector $\vec{u_i}$ in the non-rotating reference frame can be transformed to a vector $\vec{u_b}$ in the body frame using the orthogonal rotation matrix C_i^b.

$$\vec{u_b} = C_i^b \vec{u_i} \tag{2.2}$$

The elements of the direction cosine matrix (DCM) represent the projections of unit vectors in the non-rotating reference frame onto the rotating frame. For example, element 12 of the DCM represents the cosine of the angle between the X_A axis of the reference frame and the Y_B axis of the rotating frame. Similar to the attitude rate equations, the attitude propagation equation is given by the time rate of change of the rotation matrix

$$\dot{C}_i^b = -\Omega_{ib} C_i^b \tag{2.3}$$

$$\Omega_{ib} = \begin{bmatrix} 0 & -\omega_z & \omega_y \\ \omega_z & 0 & -\omega_x \\ -\omega_y & \omega_x & 0 \end{bmatrix} \tag{2.4}$$

where again ω_x, ω_y and ω_z are the x, y and z components of angular velocity of the rotating frame with respect to the reference frame. With a known initial orientation and measurements of ω_x, ω_y and ω_z from gyroscopes, the above differential equation can be integrated to determine the current orientation. Direction cosine matrices obtained using numerical integration lose their orthonormal properties due to numerical errors and require re-orthogonalization. The re-orthogonalization is usually performed at a much slower rate when compared to the integration interval. The relationship between the rotation matrix and Euler angles is given by

$$C_i^b = \begin{bmatrix} \cos\theta\cos\psi & \cos\theta\sin\psi & -\sin\theta \\ -\cos\phi\sin\psi + \sin\phi\sin\theta\cos\psi & \cos\phi\cos\psi + \sin\phi\sin\theta\sin\psi & \sin\phi\cos\theta \\ \sin\phi\sin\psi + \cos\phi\sin\theta\cos\psi & -\sin\phi\cos\psi + \cos\phi\sin\theta\sin\psi & \cos\phi\cos\theta \end{bmatrix} \tag{2.5}$$

To compute the Euler angles ϕ, θ and ψ from the rotation matrix, the following equations are used:

$$\phi = \tan^{-1}\frac{C_{23}}{C_{33}} \tag{2.6}$$

$$\theta = \sin^{-1} C_{13} \tag{2.7}$$

$$\psi = \tan^{-1}\frac{C_{12}}{C_{11}} \tag{2.8}$$

2.2.3 Axis-Angle

The orientation between the two reference frames can also be represented using the axis-angle representation. This representation is based on Euler's rotation theorem that two orthogonal frames can be made to coincide by performing a right-handed rotation about a space-fixed axis. Although the axis of rotation and the angle are not obvious, this representation is still useful in some applications such as tracking. If $R_n(\phi)$ is the rotation matrix used to align the non-rotating reference frame with the rotating frame, the angle of rotation is ϕ and the direction of rotation axis is specified by $\vec{n}$, the rotation matrix can be written as

$$R_n(\phi) = (1 - \cos\phi)nn^T + \cos\phi I_3 + \sin\phi\overline{n} \tag{2.9}$$

with $\overline{n}$ is the skew-symmetric matrix given by

$$\overline{n} = \begin{bmatrix} 0 & -n_3 & n_2 \\ n_3 & 0 & -n_1 \\ -n_2 & n_1 & 0 \end{bmatrix} \tag{2.10}$$

For the rotation operator C_i^b, the axis of rotation $\vec{n}$ is the eigenvector corresponding to the eigenvalue of +1. Therefore, the unit vector $\vec{n}$ can be determined using

$$\left[C_i^b - I\right]\vec{n} = 0 \tag{2.11}$$

The angle of rotation ϕ can be determined using the equation

$$\phi = \cos^{-1}\frac{Tr(C_i^b) - 1}{2} \tag{2.12}$$

where $Tr(C_i^b)$ is the trace of the rotation matrix. Although the axis-angle representation reduces the number of independent variables to four - the rotation angle and the three elements of the rotation axis, the rotation metrix $R_n(\phi)$ still needs to be constructed to apply a rotation. As a result, problems such as loss of orthogonality in direction cosine matrices still exist in the axis-angle representation.

2.2.4 Quaternions

Sir William R.Hamilton invented the hypercomplex numbers of rank 4 and termed them *quaternions.* Hamilton defined quaternions as 4-tuples of real numbers

$$q = (q_0, q_1, q_2, q_3) \tag{2.13}$$

Here q_0 is the scalar part of the quaternion and $\overline{q} = (q_1, q_2, q_3)$ is the vector part constructed using the standard basis vectors $\vec{i}$, $\vec{j}$ and $\vec{k}$. Quaternions, being hypercomplex numbers of rank greater than 2, do not satisfy field properties of real numbers - quaternion products are, in general, not commutative. The norm of a quaternion is defined as

$$||q|| = \sqrt{q_0^2 + q_1^2 + q_2^2 + q_3^2} \tag{2.14}$$

If the norm of the quaternion is unity, it is referred to as a unit quaternion. Just like the rotation matrix, a unit quaternion (or any quaternion in general) can be used to rotate a vector from a non-rotating reference frame to a rotating frame. For a vector $\vec{u}$, the rotation operator in terms of quaternion is expressed as [19]

$$L(q) = q^* \otimes u \otimes q \tag{2.15}$$

where

$$q^* = \begin{bmatrix} q_0 \\ -\overline{q} \end{bmatrix} \tag{2.16}$$

is the inverse of the unit quaternion q and $\otimes$ denotes a quaternion product. *L(q)* can be interpreted as an operator that rotates the reference frame A into the rotating frame B. In terms of the axis-angle rotation, if the unit quaternion q is represented as

$$q = \cos\phi + \vec{u}\sin\phi \tag{2.17}$$

the quaternion operator *L(q)* rotates the frame through an angle of 2θ. In terms of the Euler angles ϕ, θ and ψ, the component quaternions can be represented as

$$\vec{q_\phi} = \begin{bmatrix} \cos\frac{\phi}{2} \\ \sin\frac{\phi}{2} \\ 0 \\ 0 \end{bmatrix} \tag{2.18}$$

$$\vec{q_\theta} = \begin{bmatrix} \cos\frac{\theta}{2} \\ 0 \\ \sin\frac{\theta}{2} \\ 0 \end{bmatrix} \tag{2.19}$$

$$\vec{q_\psi} = \begin{bmatrix} \cos\frac{\psi}{2} \\ 0 \\ 0 \\ \sin\frac{\psi}{2} \end{bmatrix} \tag{2.20}$$

The quaternion q for the rotation operator *L(q)* can be derived from the component quaternions as

$$\vec{q} = \vec{q_\psi} \otimes \vec{q_\theta} \otimes \vec{q_\phi} \tag{2.21}$$

The elements of q can be represented in terms of the Euler angles as

$$q_0 = \cos\frac{\psi}{2}\cos\frac{\theta}{2}\cos\frac{\phi}{2} + \sin\frac{\psi}{2}\sin\frac{\theta}{2}\sin\frac{\phi}{2} \tag{2.22}$$

$$q_1 = \cos\frac{\psi}{2}\cos\frac{\theta}{2}\sin\frac{\phi}{2} - \sin\frac{\psi}{2}\sin\frac{\theta}{2}\cos\frac{\phi}{2} \tag{2.23}$$

$$q_2 = \cos\frac{\psi}{2}\sin\frac{\theta}{2}\cos\frac{\phi}{2} + \sin\frac{\psi}{2}\cos\frac{\theta}{2}\sin\frac{\phi}{2} \tag{2.24}$$

$$q_3 = \sin\frac{\psi}{2}\cos\frac{\theta}{2}\cos\frac{\phi}{2} - \cos\frac{\psi}{2}\sin\frac{\theta}{2}\sin\frac{\phi}{2} \tag{2.25}$$

Poisson's kinematic equation in quaternion form that relates the rate of change of the attitude quaternion to the angular rate of the body frame with respect to inertial frame is given by:

$$\dot{q} = \frac{1}{2} q \otimes \omega_{ib} \tag{2.26}$$

In matrix form this equation can be written as

$$\dot{q} = \frac{1}{2} * \begin{bmatrix} q_0 & -\overline{q} \\ \overline{q} & q_0 I_3 + S(\overline{q}) \end{bmatrix} \begin{bmatrix} 0 \\ \omega_{ib} \end{bmatrix} \tag{2.27}$$

where $S(\overline{q})$ is the skew-symmetric matrix

$$S(\overline{q}) = \begin{bmatrix} 0 & -q_3 & q_2 \\ q_3 & 0 & -q_1 \\ -q_2 & q_1 & 0 \end{bmatrix} \tag{2.28}$$

If q_1 and q_2 are two quaternions, the relative orientation or the error quaternion between the two is given by

$$\tilde{q} = q_1 \otimes q_2^* \tag{2.29}$$

Two frames whose attitude quaternions with respect to a reference frame are q_1 and q_2 coincide if:

$$\tilde{s} = 1 \tag{2.30}$$

$$\tilde{v} = 0 \tag{2.31}$$

where $\tilde{s}$ and $\tilde{v}$ are the real and vector parts of the quaternion error. Regardless of the magnitude of the quaternion error, $\tilde{v} = 0$ is a sufficient condition for the two frames to coincide.

2.2.5 Rodrigues Parameters

Another attitude representation related to quaternions is the Rodrigues vector, also called Gibbs vector. The parameter set is defined as [24]:

$$\vec{\rho} = \frac{\vec{q}}{q_0} = \tan\left(\frac{\theta}{2}\right)\hat{n} \tag{2.32}$$

The components (ρ_1, ρ_2, ρ_3) are referred to as the Rodrigues parameters and the quaternion in terms of these parameters is given by

$$q = \frac{1}{\sqrt{1+|\rho|^2}} \begin{bmatrix} 1 \\ \vec{\rho} \end{bmatrix} \tag{2.33}$$

Rodrigues vector is a minimum parameter set for attitude representation but rotations passing through π cannot be represented as $|\rho| \to \infty$.

2.3 Survey of Attitude Estimation

Attitude estimation has been studied extensively. Different sensor sets and techniques have been developed to estimate vehicle attitude, both online and offline. The basic sensor measurements used are

- Gyroscopes.
- Accelerometers.
- Magnetometers.
- Air data sensors.
- GPS.
- Combinations of these.

In strapdown systems attitude estimation involves estimating the orientation of a body-fixed, rotating frame with respect to an inertial frame. Wahba [27] proposed that, given measurements of two non-colinear vectors, one in a body fixed frame v_b, and one in an inertial frame, v_i, a least-squares estimate of the rotation matrix can be computed by reducing the error between the reference vector set and the rotated vector set from the body-fixed frame. The objective in this case is to find the orthogonal matrix M such that

$$\sum_{i=1}^{n} ||v_i - Mv_b||^2$$

is minimized.

Various algorithms and methods that use inertial sensors are available in the literature. A simple attitude estimation scheme for a small autonomous helicopter utilizing a two-axis inclinometer, triad of rate gyros and a compass is proposed in [3]. The inclination and the integrated outputs are combined with a complementary filter and the bandwidth of the filters are tuned to match the bandwidth of interest. A gyro-free system using non-colinear vector measurements to compute the attitude quaternion is proposed in [10]. Body frame measurements obtained from accelerometers and magnetometers are combined with the reference magnetic and gravity vectors using least-squares and a time-varying Kalman filter. The magnetic model requires the current position from a GPS and the gravitational field of the earth is assumed to be a constant and pointing down in the local vertical frame. In [11], GPS is used to determine the attitude solution using an ultra short-baseline in a triple antenna configuration, with the resulting attitude uncertainties being less than 0.5 deg. This carrier phase detection algorithm requires precise initialization to account for integer ambiguities and is sensitive to noise. It is also shown that reducing the spacing degrades the accuracy of the computed attitude solution. To coast through GPS outages and get a higher bandwidth output, inertial aiding using solid-state rate gyros is also explored. A drawback of a GPS-based attitude determination is the susceptibility to interference and loss of lock requiring reinitialization. Two recursive algorithms to solve the vector-matching problem by determining the minimum variance estimate of the attitude quaternion are presented in [5]. An extended Kalman filter is used to estimate the difference between the true attitude quaternion and the estimate. A similar recursive scheme to solve the two-vector problem using Euler angles is presented in [4].

A novel approach is taken in [20], wherein, instead of carrier phase measurements from GPS, signal-to-noise (SNR) measurements are used to determine three-axis attitude. The SNR measurements and the gain pattern of the antenna are used to compute the orientation of the platform. When compared to the conventional carrier-phase estimation, this method has the advantage of requiring no reinitialization. However, the sensitvity in yaw is dependent on the antenna geometry and hence the possibility of combining the standard carrier-phase method with the SNR measurements is also explored.

Another approach, utilizing GPS velocity signals to generate a 'pseudo-attitude' for general aviation applications, is presented in [13]. Velocity measurements from a single GPS antenna are used to synthesize flight path angle relative to the local horizontal plane and the roll angle about the velocity vector, assuming non slipping turns. It is shown that the body axes and the wind axes are closely oriented, and the synthesized attitude is closely related to the conventional pitch and roll angles. The computed 'pseudo-attitude' is suitable for backup attitude indicators. A fast estimation algorithm to solve the vector matching problem using quaternions is proposed in [21]. Complementary filtering schemes that take advantage of the short-term stability of the gyros and the long-term stability of accelerometers are also popular. A fuzzy logic signal processing approach to adaptively adjust the filter bandwidths to correct the gyro bias is proposed in [22].

2.4 Complementary filtering

Complementary filtering is a technique used to combine measurements from two or more sources with different spectral characteristics with minimal distortion in the signal output.

The measurement sources usually have different frequency regions where the measurement is reliable - hence the term complementary filter. Figure 2.2 below shows the basic block diagram of a complementary filter[7].

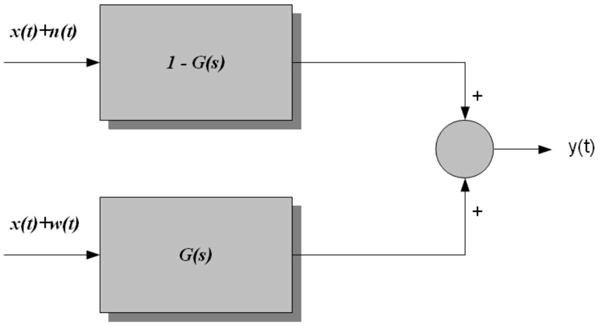

Figure 2.2: Complementary filter

The signal $x(t)$ to be extracted is measured by two sources with complementary spectral characteristics. Measurements from one source are more reliable at high frequencies whereas the measurement from the other source is accurate at low frequencies. Combining the two measurements by passing the first measurement through a high pass filter - represented by the transfer function $1 - G(s)$, and the second measurement through a low pass filter $G(s)$ represents the basic idea behind complementary filtering. The signal $x(t)$ is unaffected in this scheme, whereas the noise from the two sources is shaped differently by the filters. The output signal $y(t)$ can be represented as

$$Y(s) = \big[X(s) + N(s)\big]\big[1 - G(s)\big] + \big[X(s) + W(s)\big]G(s) \tag{2.34}$$

or

$$Y(s) = X(s) + N(s)\big[1 - G(s)\big] + W(s)G(s) \tag{2.35}$$

With this scheme, the problem reduces to determining the transfer function $G(s)$ to shape the spectral characteristics of the two sources to provide the best estimate of $x(t)$. The idea can be extended to include more than two sources by making the transfer function of one path the complement of the sum of the other two transfer functions. As an application of complementary filtering to single-axis attitude estimation - given measurements y_1 and y_2 from an inclinometer and a rate gyroscope respectively, the estimate for the tilt $\theta(t)$ can be written as

$$\theta(t) = G(s)Y_1(s) + \big[1 - G(s)\big]Y_2(s) \tag{2.36}$$

2.5 SO(3) complementary filtering

The term SO(3) refers to the special orthogonal group - the group of all orthogonal matrices that represent a rotation in 3D space. The principles of complementary filtering have been extended by various authors to design nonlinear controller/observers in rigid bodies. An earlier work by [25] presents a design of a nonlinear velocity and angular momentum observer for rigid bodies using Euler quaternions and energy functions. Angular velocity estimates are generated using torque and orientation measures and the exponential convergence of the observer is demonstrated. Reference [14] extends the nonlinear angular velocity observer to estimate bias, scale factor and misalignment errors in gyros and accelerometers. The residual bias errors in the gyro measurements are assumed to decay exponentially. The angular velocity observer presented in [25] and [14] requires a true attitude quaternion and the residual bias, scale factor errors etc. are estimated using the observed attitude errors. The observer proposed in [14] is of the form

$$\begin{bmatrix} \hat{q}_0 \\ \hat{\bar{q}} \end{bmatrix} = \frac{1}{2} \begin{bmatrix} -\hat{q}_0{}^T \\ \hat{q}_0 I + S(\hat{\bar{q}}) \end{bmatrix} \Big[(I + \hat{\Delta}\omega_{imu} + \hat{b} + K\mathrm{sgn}(\tilde{s})\tilde{v}\Big] \tag{2.37}$$

$$\dot{\hat{b}} = -\beta\hat{b} + \frac{1}{2}\mathrm{sgn}(\tilde{s})\tilde{v} \tag{2.38}$$

where $\hat{b}$ is the estimated gyro bias, $[\hat{q}_0 \quad \hat{\bar{q}}]$ is the estimate of the attitude quaternion and $[\tilde{s} \quad \tilde{v}]$ are the real and the vector parts of the quaternion error.

The angular velocity observer in [14] is shown to be exponentially stable with the equilibrium points $(0, 0, 0)$ and $(\pm 1, 0, 0, 0)$ for the bias errors and attitude quaternion respectively. [18] proposes a similar algorithm to estimate a constant bias in angular velocity measures. The bias estimates are used as part of a nonlinear algorithm for spacecraft attitude control. The observer proposed for gyro bias is of the form

$$\dot{\hat{q}} = \frac{1}{2}Q(\hat{q}(t))R^T(\tilde{s})\left[\hat{\omega}(t) + k\text{sgn}(\tilde{s}(t))\tilde{v}(t)\right] \tag{2.39}$$

$$\dot{\hat{b}}(t) = -\frac{1}{2}\text{sgn}(\tilde{s}(t))\tilde{v}(t) \tag{2.40}$$

[12] proposes a complementary filter design using rotation matrices, instead of attitude quaternion, for control of unmanned aerial vehicles. A cost function E_t of

$$E_t = \frac{1}{2}tr(I - \tilde{R}) = 2\sin^2(\frac{\theta}{2}) \tag{2.41}$$

is used to show exponential convergence. The proposed observer kinematics is of the form

$$\dot{\hat{R}} = (R\Omega + \hat{R}\omega(R, \hat{R}))_x\hat{R} \tag{2.42}$$

where

$$\omega = k_{est}\text{vex}(\pi_a(\tilde{R})) \tag{2.43}$$

with vex() defined as the operation to convert the skew-symmetric rotation error matrix $\tilde{R}$ into an error vector. This operation is the inverse of the operation below that converts a vector $\vec{\omega}$ to a skew-symmetric matrix Ω_x.

$$\vec{\omega} \times \vec{a} = \Omega_x \vec{a} \tag{2.44}$$

In the above equations R is the true attitude matrix obtained from another source - accelerometers and magnetometers, for example. Using the corrected attitude matrix $\hat{R}$ to transform Ω simplifies the observer equation to

$$\dot{\hat{R}} = \hat{R}(\Omega + \omega)_x \tag{2.45}$$

with ω again given by

$$\omega = k_{est}\text{vex}(\pi_a(\tilde{R})) \tag{2.46}$$

If R is the reference attitude matrix and $\hat{R}$ is the last known estimate of the filter, the attitude error required to compute ω can be computed as the relative orientation between the two frames:

$$\tilde{R} = \hat{R}^T R \tag{2.47}$$

The ω term in the above equations can be viewed as the rate correction in the body frame necessary for the attitude matrix $\hat{R}$ to track the true attitude R. For a constant gyro bias, the observer kinematic equation using a quaternion representation is written as [12]

$$\dot{\hat{q}} = \frac{1}{2}\hat{q} \otimes p(\Omega - \hat{b} + \omega) \tag{2.48}$$

with

$$\dot{\hat{b}} = -k_b \tilde{s}\tilde{v} \tag{2.49}$$

and

$$\omega = k_{est}\tilde{s}\tilde{v} \tag{2.50}$$

where $\tilde{s}$ and $\tilde{v}$ are the real and the vector parts of the quaternion error.

2.6 Fuzzy logic

Fuzzy logic provides a method to represent control strategies as if it were implemented by a human. Fuzzy control methods attempt to implement a human being's intuitive knowledge to achieve the desired controlled outputs. Reference [23] provides an excellent reference on the design of fuzzy controllers. The basic building blocks of a fuzzy controller are:

- Fuzzifier.
- Inference block.
- Rule Base.
- Defuzzifier.

Figure 2.3 below shows the basic block diagram of a generalized fuzzy logic controller with a set of inputs, rule base and outputs[7].

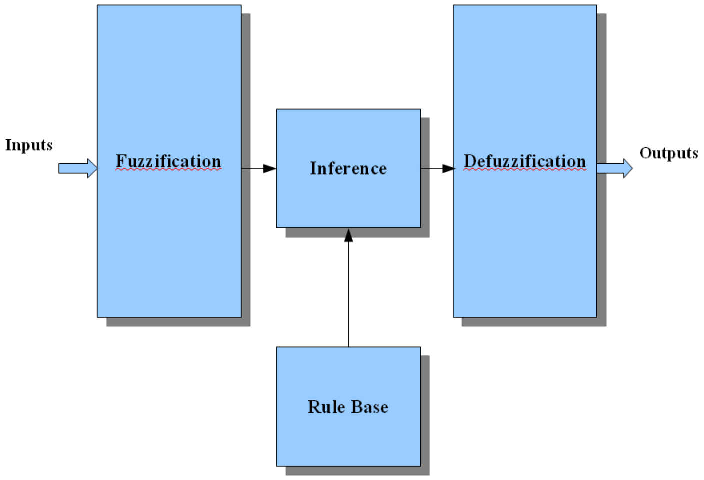

Figure 2.3: Fuzzy Control Building Blocks

As shown in the above figure, external inputs are converted by the fuzzifier, using a set of if-then rules, into different input classes such as ‘negative large’, ‘negative small’, ‘positive small’ etc., to create the input membership function set. Each input - usually an ‘error’ measure $e(t)$ and a ‘rate of change of error’ measure $\dot{e}(t)$, is processed by the fuzzifier. For example, triangular membership functions for an ‘error’ input $e(t)$ are shown in Figure 2.4.

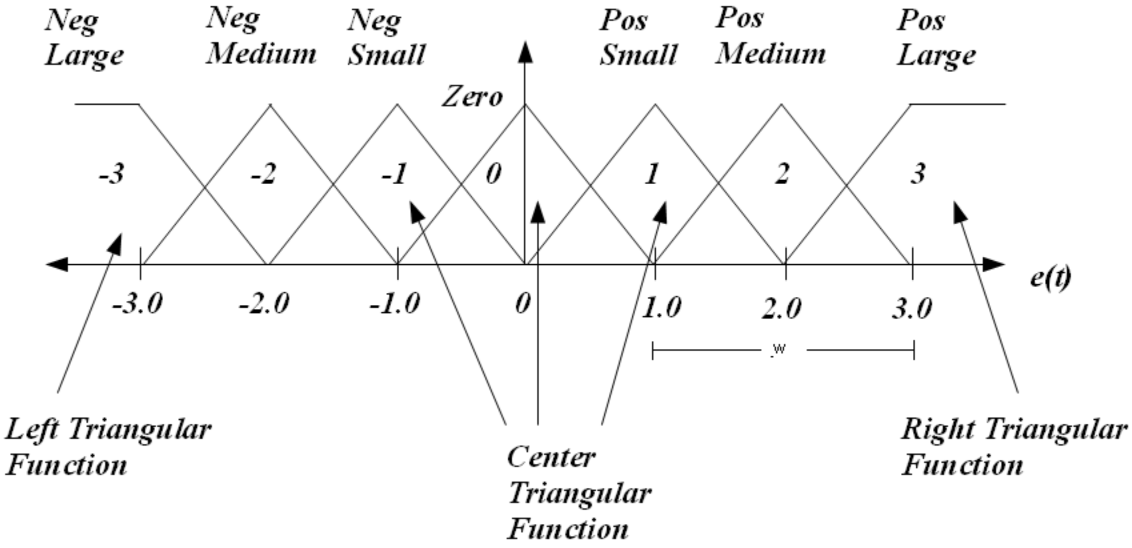

Figure 2.4: Fuzzy Membership Function

The set of physical values that an input can assume is referred to as the ‘universe of discourse’ for the input parameter. Each triangular membership function has a center(c) and a width(w) that determine the probability that a given input belongs that membership function. For example, an input error of 1.5 in Figure 2.4 would belong to both “positive small” and “positive medium” membership functions. The fuzzifier determines the certainty (a measure of probability) that the input belongs to a group of membership functions or the certainty that a particular rule is applicable. If u is the input, the certainty for the triangular membership functions with center(c) and a width(w) can be determined using the following equations [23]:

Left Triangular Membership Function

$$y = \begin{cases} 1.0 & \text{if } u \leq c \\ \max\bigl(1 - \frac{u-c}{0.5w}, 0\bigr) & \text{if } u > c \end{cases}$$

Right Triangular Membership Function

$$y = \begin{cases} \max\bigl(1 + \frac{u-c}{0.5w}, 0\bigr) & \text{if } u \leq c \\ 1.0 & \text{if } u > c \end{cases}$$

Center Triangular Membership Function

$$y = \begin{cases} \max\bigl(1 + \frac{u-c}{0.5w}, 0\bigr) & \text{if } u \leq c \\ \max\bigl(1 - \frac{u-c}{0.5w}, 0\bigr) & \text{if } u > c \end{cases}$$

Once the applicability of all the input rules is determined, a 'confidence matrix' for all combinations of inputs is generated. For example, if μ_e is the certainty associated with 'error' and $\mu_{\dot{e}}$ is the certainty associated with 'rate of error', then the combined certainty that both the rules apply is given by

$$\mu = \mu_e \times \mu_{\dot{e}} \tag{2.51}$$

The rule base matrix is a set of rules that specify the output values for each input combination. The confidence matrix is scaled element-by-element with the rule base in the defuzzification step and the entries are summed to generate the controller output.

Chapter 3

MEMS Sensor Modeling and Calibration

3.1 Overview

Usage of MEMS sensors in inertial sensing relies heavily on characterizing the behavior of the sensor and developing compensation techniques to correct the device outputs. Depending on the application, the compensation can be applied in real-time or offline. This chapter describes the sensor models used in this work for MEMS gyros, accelerometers and magnetometers and an overview of calibration methods to reduce the deterministic errors. Stochastic models of gyros and accelerometers are developed to understand the performance limits of the sensors and the underlying noise characteristics. The parameters from the stochastic models are used in the development of an extended Kalman filter. In addition, the parameters are used as an aid to determine the correction gains in the proposed algorithm.

3.2 Operation of MEMS Gyroscopes

Angular rate MEMS sensors use the Coriolis effect on a proof mass to sense angular motion. A vibrating proof mass with a linear velocity of $\vec{v}$ which is subjected to an angular rate of Ω experiences a Coriolis acceleration given by

$$A_c = -2(\vec{\Omega} \times \vec{v}) \tag{3.1}$$

The acceleration is perpendicular to the rotational axis and the velocity. For example, ADXRS150 is a vibratory MEMS gyro that uses the Coriolis effect. Angular rate measurement range of several thousand degrees per second has been achieved with this technology.

Quartz-based and resonant ring MEMS gyroscopes are other MEMS gyro technologies that use similar vibratory elements. MEMS accelerometers rely on sensing the displacement of a proof mass leading to a change in capacitance or a change in frequency of a vibrating beam subjected to a linear acceleration. The advantages of silcon sensors outweigh the drawbacks that accompany reduction in size such as decreased sensitivity, resolution, increased noise and thermal sensitivity etc.[9].

3.3 MEMS Gyro Error Sources

MEMS gyroscopes have a number of errors that corrupt the angular rate measurement. The errors can be classified as deterministic and stochastic. Deterministic errors that corrupt a gyro measurement include:

- Scale factor errors.
- Thermal variation of bias.
- Linear acceleration sensitivity.

The scale factor (S_f) of a MEMS gyro can exhibit variation with temperature as well as applied angular rate. The g-sensitivity term indicates that the output of the sensor can change as a function of linear acceleration. The g-sensitivity term manifests as a bias shift at the output of the sensor. The deterministic terms - scale factor errors, thermal variation of bias and g-sensitivity, can be characterized through carefully designed calibration methods. The deterministic terms in the MEMS gyroscope measurement equation - S_f, $O(T)$, and $g(A)$, can be computed using standard offline calibration techniques. For an orthogonal triad of gyroscopes, sensor readings collected at different temperatures with a null input angular rate can be used to determine the variation of bias with temperature. MEMS gyroscopes usually provide a sensor core temperature output and this can be used to compensate bias variation with temperature. A polynomial fit of the readings against the recorded temperature can compensate for the variation. The scale factor matrix can be determined by spinning the orthogonal triad at different temperatures. A 2D surface fit of the collected readings against rate and temperature gives the scale factor matrix. If the scale factor dependence on temperature is minimal, a curve fit will suffice. G-sensitivity matrix can be determined by subjecting the gyroscope to linear accelerations along the three orthogonal axes. Gravitational acceleration can be used as the input to determine the g-sensitivity coefficients.

The stochastic errors that corrupt a gyroscope measurement can be classified into the following categories:

- Angle Random Walk
- Bias Instability.
- Rate Random Walk.
- Exponentially Correlated Noise.

In addition to the above errors, a random constant turn-on bias can also corrupt the measurement. The turn-on bias can be estimated at startup by averaging a long sequence (typically 1 to 3 minutes) of gyro measurements. To characterize the other stochastic errors, techniques like Allan Variance and autocorrelation are used. Allan Variance is a time domain data analysis technique developed by David Allan to study the frequency stability of oscillators[2]. The analysis has since been extended to study random processes in data sets and can be used to identify noise sources. The following sections briefly describe the stochastic errors and the methods to estimate them.

3.3.1 Angle Random Walk

Angle random walk(ARW) is a measure of the wideband noise η with correlation time shorter than the sampling period. MEMS gyroscopes are usually bandlimited with a pre-sampling filter and hence the wideband noise spectrum can be assumed to be ‘white’ when compared to the device bandwidth. Wideband noise at the output of the sensor causes the integrated attitude solution to exhibit a ‘random walk’ behavior. Random walk is characterized by a standard deviation that increases with $\sqrt{t}$. The rate noise power spectral density as a function of frequency f can be represented by [1]

$$S_{\omega}(f) = N^2 \tag{3.2}$$

where N is the angular random walk coefficient. The relationship between the Allan Variance of wideband noise and the ARW coefficient is given by

$$\sigma^2(\tau) = \frac{N^2}{\tau} \tag{3.3}$$

where τ is the averaging time. The above equation indicates that at $\tau = 1$, the ARW coefficient is equal to $\sigma(\tau)$ and a log-log plot of $\sigma(\tau)$ versus τ will have a slope of -1/2. Figure 3.1 shows a comparison of Allan variance of simulated noise sources with variances - 0.1, 0.25 and 0.5. An increase in the noise variance moves the log-log plot upward resulting in a higher ARW coefficient, indicating that the random walk in the integrated output will be higher. The ARW coefficient is usually expressed in deg/$\sqrt{hr}$.

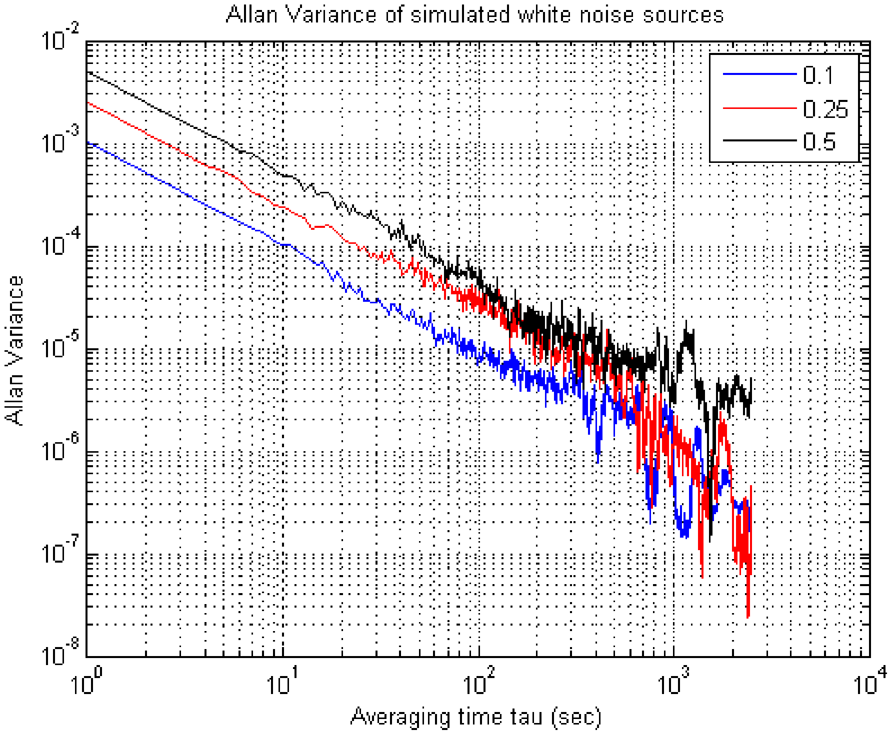

Figure 3.1: Comparison of Allan Variance of Simulated White Noise Sources

3.3.2 Bias Instability

Bias instability, usually expressed in deg/hr, represents a fundamental performance limitation of a MEMS gyro - it is the minimum uncertainty in the estimated bias that can be achieved with a fully modeled sensor. Bias instability is associated with *1/f* noise in the electronics and has a rate PSD given by[1]

$$S_\omega(f) = \begin{cases} \frac{B^2}{2\pi}\frac{1}{f} & \text{if } f \le f_0 \\ 0 & \text{if } f > f_0 \end{cases}$$

The log-log Allan deviation plot has a slope of +1 for smaller averaging times and a slope of 0 for higher values of τ. The zero-slope region can be used to determine the bias instability of the sensor.

3.3.3 Rate Random Walk

Rate random walk is associated with $1/f^2$ noise with the rate PSD given by:

$$S_\omega(f) = \frac{K}{2\pi}^2 \frac{1}{f^2} \tag{3.4}$$

with K being the rate random walk coefficient. The Allan deviation plot shows a slope of +1/2. In a similar fashion, the rate ramp and quantization errors show slopes of +1 and -1 respectively. Rate random walk and rate ramp indicate processes that have increasing variance and are physically unrealizable.

3.3.4 Exponentially Correlated Noise

An exponentially correlated (or Gauss-Markov) process is a stationary process with an exponentially decaying autocorrelation. The rate PSD of a Gauss-Markov process

$$S(\omega) = \frac{2\sigma^2\beta}{\omega^2 + \beta^2} \tag{3.5}$$

where σ^2 and $1/\beta$ are mean-square value and the time constant of the process.

The autocorrelation of the process is given by:

$$R(\tau) = \sigma^2 e^{-\beta|\tau|} \tag{3.6}$$

The Allan Variance of a Gauss-Markov process converges to that of ARW for averaging times much greater than $1/\beta$. For averaging times much smaller than $1/\beta$, the Allan variance approaches a rate random walk. A Gauss-Markov process is usually used as an approximation for a rate random walk. A Gauss-Markov sequence is generated using the equation:

$$X_{k+1} = e^{-\beta\delta t} X_k + W_k \tag{3.7}$$

where W_k is the driving white noise sequence with zero mean and variance equal to $\sigma^2[1 - e^{-2\beta\Delta t}]$,

σ^2 is the variance of the Gauss Markov process,

$\beta = 1/\tau$,

and Δt is the sampling period

Figure 3.2 shows the comparison plot of Allan variance of three simulated Gauss-Markov processes with a time constant of 1000 seconds and different variances. As shown in the figure, increasing the variance of the exponential process shifts the Allan variance plot toward lower correlation times.

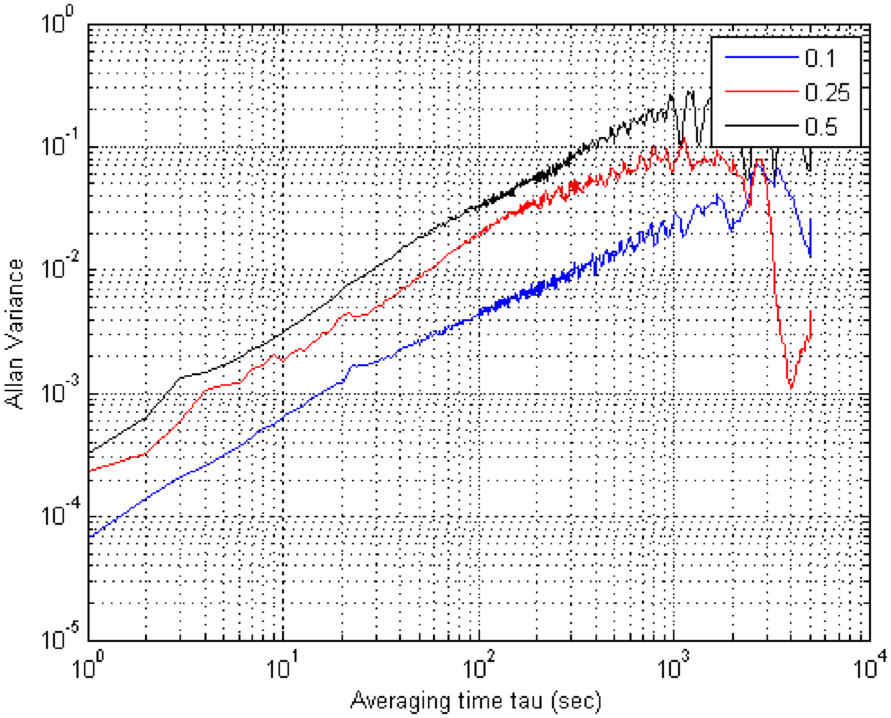

Figure 3.2: Allan Variance of simulated Gauss-Markov processes - Constant Tau

Figure 3.3 shows the comparison plot of Allan variance of three Gauss-Markov processes with a variance of 0.1 and different time constants. As shown in the figure, decreasing the time constant makes the plot look more like angular random walk.

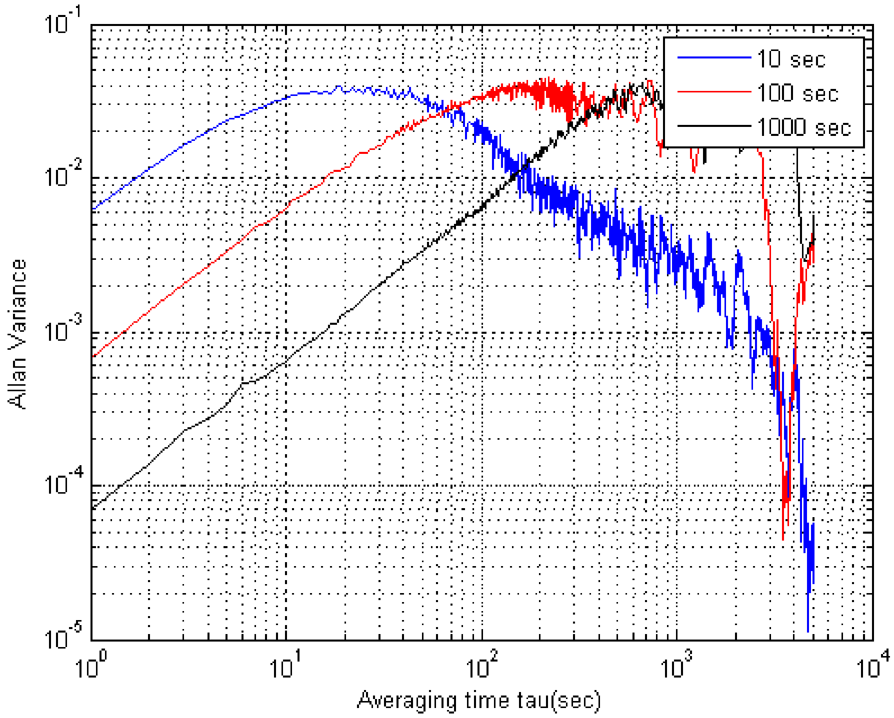

Figure 3.3: Allan Variance of simulated Gauss-Markov processes - Constant Variance

3.3.5 MEMS Gyroscope Model

From the discussion of the error sources in the previous section, the measurement model for a MEMS gyroscope can be written as

$$M = S_f(T,\omega)\omega + O(T) + g(A) + b_{dc} + b_i(t) + \eta_w \tag{3.8}$$

where

S_f is the scale-factor of the gyroscope,

ω is the applied angular rate,

$O(T)$ is the variation of bias as a function of temperature,

$g(A)$ is the g-sensitivity,

b_{dc} is the turn-on bias,

b_i is the time varying bias,

η is the wideband noise

For a triad of orthogonally mounted gyroscopes, the above equation can be written as

$$\begin{bmatrix} M_x \\ M_y \\ M_z \end{bmatrix} = \begin{bmatrix} S_{xx} & S_{xy} & S_{xz} \\ S_{yx} & S_{yy} & S_{yz} \\ S_{zx} & S_{zy} & S_{zz} \end{bmatrix} \begin{bmatrix} \omega_x \\ \omega_y \\ \omega_z \end{bmatrix} + \begin{bmatrix} O_x(T_x) \\ O_y(T_y) \\ O_z(T_z) \end{bmatrix} + \begin{bmatrix} g_{xx} & g_{xy} & g_{xz} \\ g_{yx} & g_{yy} & g_{yz} \\ g_{zx} & g_{zy} & g_{zz} \end{bmatrix} \begin{bmatrix} A_x \\ A_y \\ A_z \end{bmatrix} + \begin{bmatrix} b_{xdc} \\ b_{ydc} \\ b_{zdc} \end{bmatrix} + \begin{bmatrix} b_x(t) \\ b_y(t) \\ b_z(t) \end{bmatrix} + \begin{bmatrix} \eta_x \\ \eta_y \\ \eta_z \end{bmatrix} \tag{3.9}$$

where the scale factor S_f is expanded to include misalignment terms and the g-sensitivity term is expanded to include sensitivity to applied acceleration in x, y and z axes.

An exponentially correlated process model is assumed for the bias variation $b_i(t)$ with time:

$$\dot{b_i} = \frac{-1}{\tau} b_i + \eta_w \tag{3.10}$$

where τ is the time constant of the process and η_w is the driving noise.

3.3.6 Determination of Stochastic Model Parameters

To estimate the stochastic errors and the model parameters, the Allan deviation of ADXRS150 is computed with readings collected from the device at a constant temperature. The sensor readings are sampled at 100 Hz and decimated to 10 Hz. The Allan deviation of three ADXRS150 gyroscopic sensors used to generate data for this dissertation is shown in Figure 3.4.

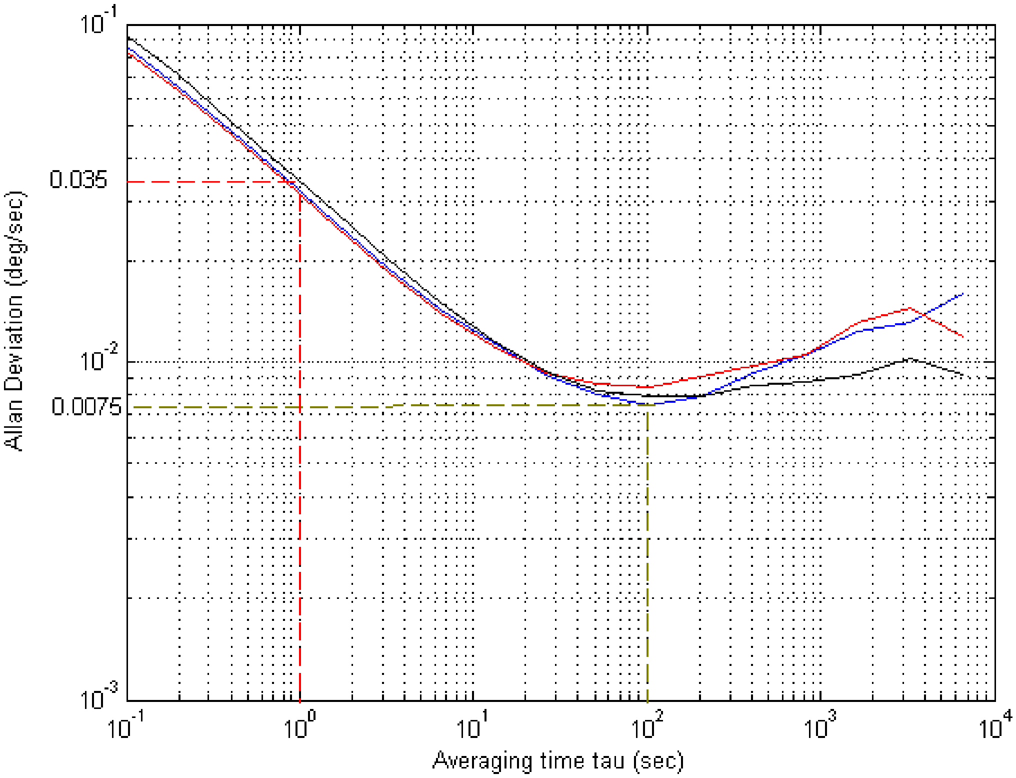

Figure 3.4: ADXRS150 Allan Deviation

The following observations are made from the Allan deviation plot:

- The ARW can be determined from this plot as the Allan deviation corresponding to $\tau = 1sec$ - approximately 0.035 deg/sec or an ARW of 2.1 deg/$\sqrt{hr}$.
- The bias stability of the gyro is the minimum Allan deviation - approximately 0.0075 deg/sec or 28 deg/hr.
- For $\tau > 100$ sec, the process can be approximated with an exponentially correlated process.

To estimate the parameters σ^2 and β of the exponentially correlated process, the autocorrelation of a lengthy time sequence of sensor readings is used. A major consideration in computing the autocorrelation is the amount of experimental data required to achieve the required accuracy. The variance of the experimental autocorrelation satisfies[7]

$$\mathrm{Var}V_x(\tau) \leq \frac{4}{T}\int_0^\infty {R_x}^2(\tau)d(\tau) \tag{3.11}$$

For a Gauss-Markov process with exponential autocorrelation this reduces to

$$\mathrm{Var}V_x(\tau) \leq \frac{2\sigma^4}{\beta T} \tag{3.12}$$

Accurate determination of the autocorrelation parameters is very difficult in practice. It is shown in [7] that for a 10% accuracy, the experimental data required is 200 times the time constant of the Gauss-Markov process. Since the Allan deviation plot of ADXRS150 only showed that the time constant of the underlying process is much greater than 100 sec, determining the model parameters σ^2 and β requires a very large data set.

Figure 3.5 shows the autocorrelation computed from three ADXRS150 gyros. The readings are collected at a constant temperature and the length of the sequence is 32000 seconds. The readings are unbiased, filtered with a low pass filter to remove wideband noise and scaled with the default scale factor to convert to deg/sec.

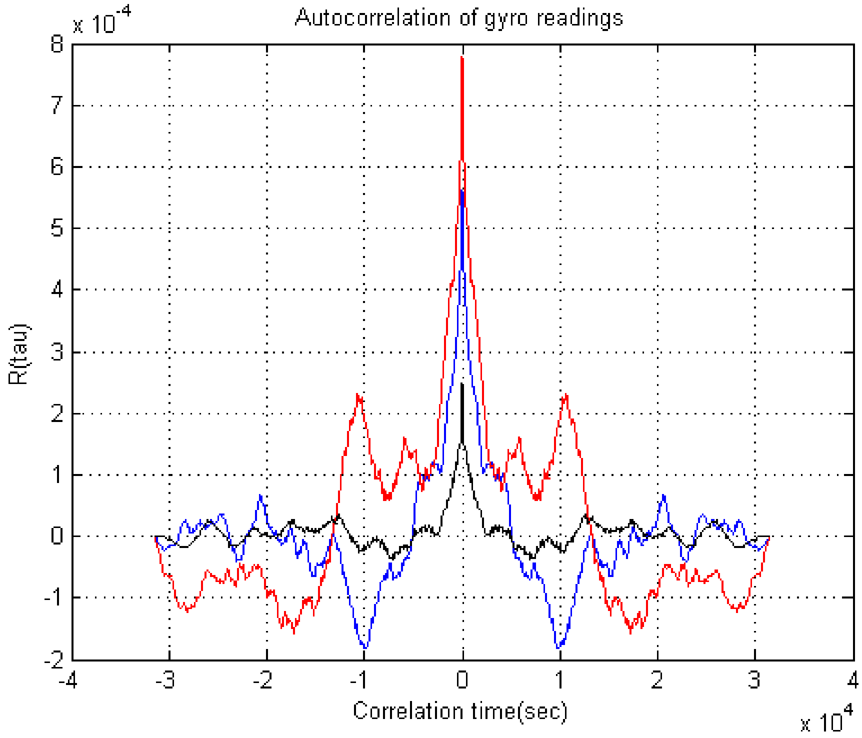

Figure 3.5: Experimental Autocorrelation

The variability in the computed autocorrelation can be seen in the above figure. To generate the model parameters σ^2 and β, an exponential fit is made on the experimental autocorrelation as shown in Figure 3.6.

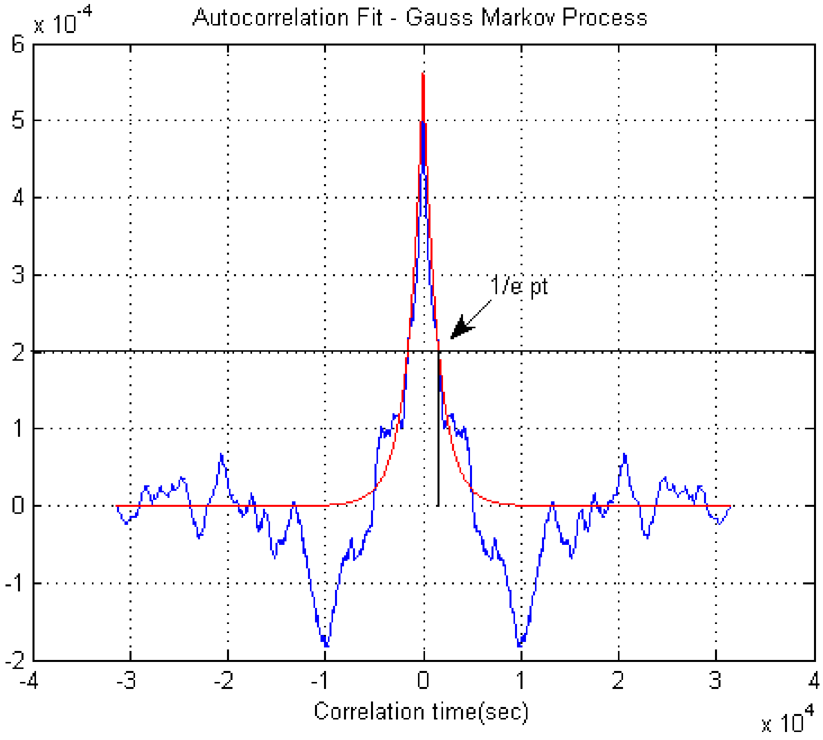

Figure 3.6: Exponential fit for autocorrelation

Due to the difficulties associated with accurate determination of the autocorrelation and the observed variability among different parts, the following values are assumed for σ^2 and $\tau(= 1/\beta)$:

- $\sigma^2 \approx 3 \times 10^{-4}\big[deg/sec\big]^2$.

- $\tau \approx 500$ sec.

3.3.7 Gyro Model Verification

In summary, the following model parameters are determined for the ADXRS150 MEMS gyroscopes used in this work. These model parameters are used in the development of the proposed algorithm in Chapter 4 and in simulation studies in Chapter 5.

- Angular random walk (Wideband noise) coefficient of 0.035 deg/sec or 2.1 deg/$\sqrt{hr}$.

- Bias Instability ≈ 28 deg/hr.
- Gauss Markov variance of $3 \times 10^{-4}[deg/sec]^2$.
- Gauss Markov time constant of 500 sec.

The gyroscopic model parameters are verified by comparing the Allan variance of the simulated gyroscopic readings with the experimental Allan variance from two ADXRS150 sensors as shown in Figure 3.7. The angular random walk and the bias stability of the simulated readings are seen to match reasonably well with the experimental readings.

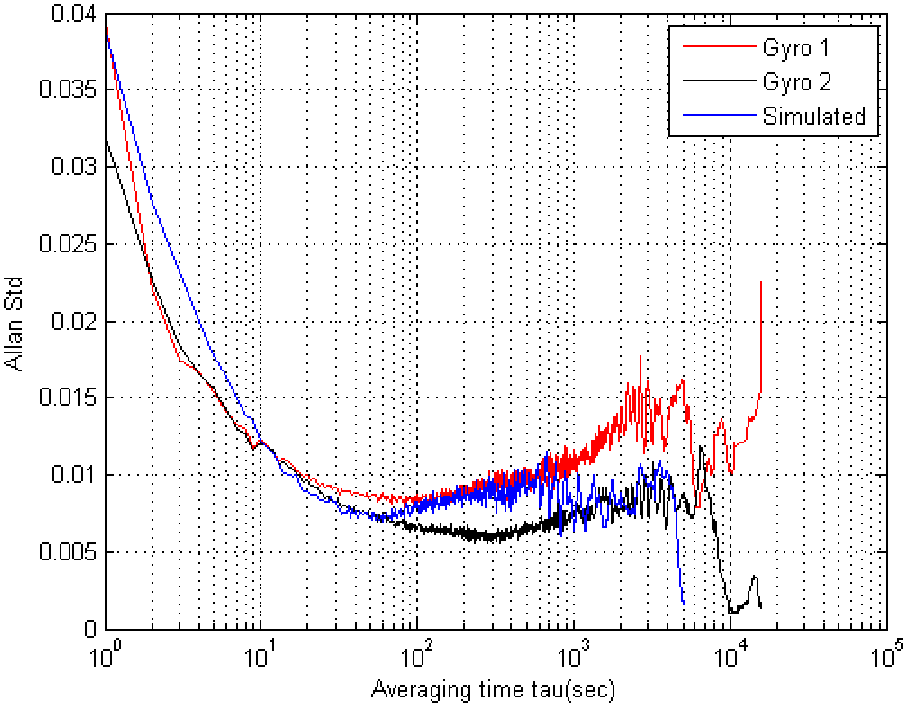

Figure 3.7: Gyro Allan Variance Comparison

3.4 MEMS Accelerometer Model

MEMS accelerometers in strapdown systems measure the specific force on a proof mass, coordinatized in the body frame. If $\vec{a_i}$ is the inertial acceleration and $\vec{g}$ is the gravity vector then the specific force is given by:

$$\vec{f} = \vec{a_i} - \vec{g} \tag{3.13}$$

The measured specific force is the component along the sensitive direction of the accelerometer and is coordinatized in the body frame.

Like gyros, MEMS accelerometers have a number of error sources that corrupt the specific force measurement. The measurement model for a MEMS accelerometer, assuming that the turn-on bias is negligible, can be written as

$$f_b = S_f(T)A + O(T) + b_{dc} + b_i(t) + \eta_f \tag{3.14}$$

where

S_f is the scale-factor of the accelerometer.
A is the applied specific force.
$O(T)$ is the variation of bias as a function of temperature.
b_{dc} is the turn on bias.
b_i is the bias variation as a function of time.
η_f is the wideband noise.

The deterministic terms - scale factor errors, thermal variation of bias and misalignment, can be characterized through calibration methods. For an orthogonal triad of accelerometers, sensor readings collected at different temperatures on a leveled surface can be used to determine the variation of bias with temperature. A measure of the sensor core temperature output can be used to compensate for the bias variation. The scale factor matrix can be determined by using gravity as the excitation or by using a centrifuge.

Turn on bias b_{dc} in an accelerometer, if not estimated, manifests as an attitude initialization error during system alignment. For small angles, the tilt errors in the roll and pitch axes introduced by the accelerometer biases [9] can be expressed as

$$\delta\alpha = \frac{-B_y}{g} \tag{3.15}$$

$$\delta\beta = \frac{B_x}{g} \tag{3.16}$$

where $\delta\alpha$ is the initialization error in roll angle, $\delta\beta$ is the initialization error in pitch angle and B_x, B_y are the biases of the x and y-axis accelerometers respectively. In an attitude heading reference system the gravity vector derived from the accelerometers is used as a reference, the accelerometer biases cannot be estimated without an external aiding source. In this attitude estimation study, the turn-on bias in accelerometers is assumed to be negligible.

The methods to estimate the stochastic errors in MEMS accelerometers are analogous to MEMS gyros, with the velocity random walk(VRW), bias instability and exponentially correlated noise being commonly used. Figure 3.8 shows the Allan deviation of measurements from three ADXL210 accelerometers.

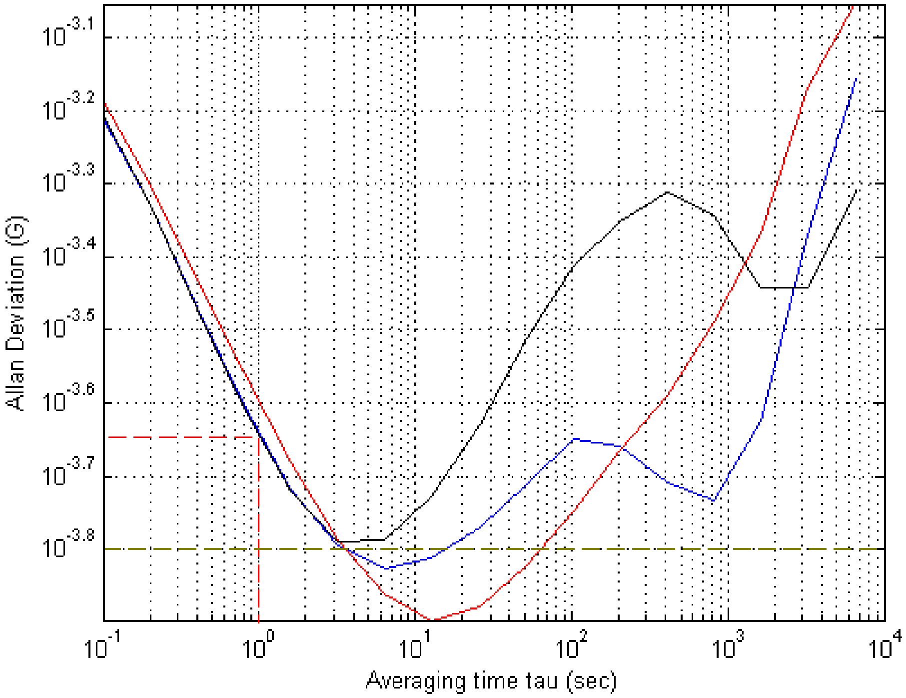

Figure 3.8: Allan deviation of ADXL210 MEMS accelerometers

From the above figure, the following values are computed:

- Velocity Random Walk (Allan deviation at $\tau = 1sec$) $\approx 10^{-3.65}G \approx 0.093$ m/sec/$\sqrt{hr}$.
- Bias instability (minimum Allan deviation) $\approx 10^{-3.8}G \approx 5.6$ m/sec/hr.
- For correlation times greater than 10 sec, the bias variation can be modeled as a Gauss-Markov process.

To compute the variance and time constant of the Gauss-Markov process, the autocorrelation approach described for the MEMS gyros is used. ADXL210 readings are collected at a constant temperature and the length of the sequence is 32000 seconds. The readings are unbiased, filtered with a low pass filter to remove wideband noise and scaled with the default scale factor to convert to units of G. Figure 3.9 shows the unfiltered and filtered readings from an ADXL210 downsampled to 1 Hz.

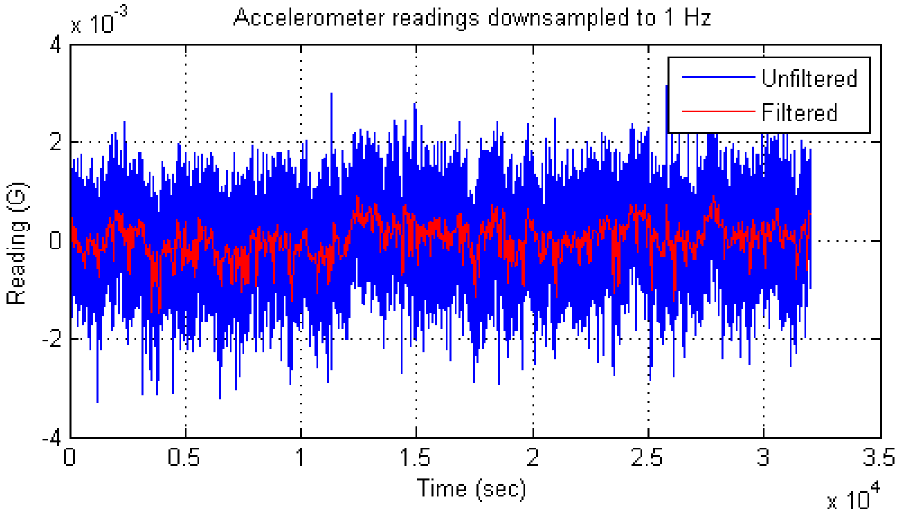

Figure 3.9: ADXL210 Experimental Readings

Figures 3.10 and Figures 3.11 show the autocorrelation of three ADXL210 accelerometers computed from filtered readings and the exponential fit, both in units of G^2.

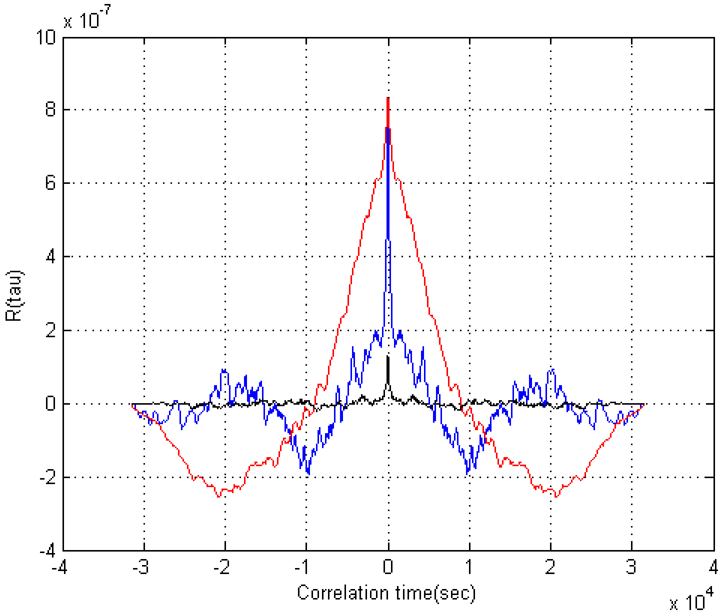

Figure 3.10: Computed Autocorrelation of accelerometers

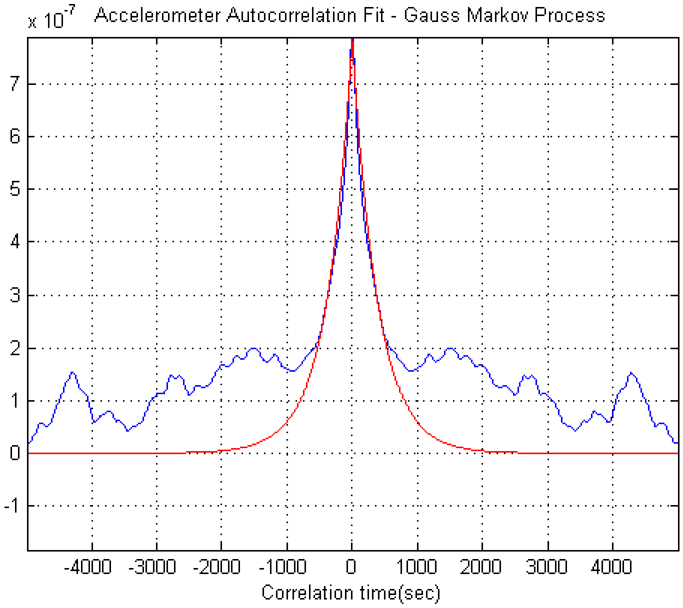

Figure 3.11: Autocorrelation fit for accelerometers

From the exponential fit Figures 3.11, the following autocorrelation parameters are computed for accelerometers:

- Gauss Markov process variance σ^2 (peak value of autocorrelation) $\approx 7 \times 10^{-7} G^2$.
- Gauss Markov process time constant τ (time value corresponding to $\frac{1}{e} \times$ peak value) ≈ 500 sec.

3.5 Magnetic Sensors

Three-axis attitude solution requires integrating the output of the rate gyros with a known initial attitude. Initial values of roll and pitch attitudes can be obtained from the gravity reference, whereas the initial heading requires a magnetic sensor or a GPS. Furthermore, to prevent an unbounded growth in attitude errors, some form of reinitialization is always required. A magnetic sensor is used in this work to compute the reference magnetic heading. Single-chip magnetic sensors, like Honeywell HMC105X, are magnetoresistive sensors that sense a change in resistance due to an applied magnetic field. Magnetoresistive sensors have the following advantages when compared to the traditional flux-gate sensors:

- Low cost and size.
- High sensitivity
- Low temperature sensitivity

Three orthogonally aligned magnetic sensors can sense the Earth's magnetic field in the body frame. If H_x, H_y and H_z are the components of the Earth's field in the magnetic north, east and the local vertical directions, then the magnetic field sensed is given by:

$$\vec{B} = C_\phi C_\theta \vec{H} \tag{3.17}$$

where C_ϕ and C_θ are the rotation matrices along the reference y and x axes respectively. Given the current roll and pitch attitudes, the measurement vector $\vec{B}$ can be transformed into the reference frame and the magnetic heading can be computed as:

$$\psi = \arctan\left[\frac{-H_y}{H_x}\right] \tag{3.18}$$

3.5.1 Magnetometer Model

Magnetic sensors measure the Earth's magnetic field at the mounted location and are thus susceptible to a number of error sources. For navigation over small distances close to the earth's surface the magnetic field vector $\vec{H}$ can be assumed to be constant, and the basic measurement model for a magnetic sensor can be written as:

$$\vec{B_b} = S_{si} S_{sf} {C_i}^b \vec{H} + \delta\vec{B}_b \tag{3.19}$$

where

$\vec{H}$ is vector $\left[H_x H_y H_z\right]^T$,

${C_i}^b$ is the direction cosine matrix from local horizontal reference frame to the body frame,

S_{si} is the matrix representing soft-iron errors,

S_{sf} is the matrix representing on and off-axis scale factors,

$\vec{B}_b$ is the vector of measures from the magnetic sensors,

$\delta\vec{B}_b$ is the vector of hard-iron offsets.

The matrix ${C_i}^b$ represents the difference in orientation between the local level reference frame and the body frame. The matrix ${C_i}^b$ is not an error source but is still required to accurately transform measures between the two frames. S_{si} is the matrix representing installation-dependent soft-iron errors. Soft-iron errors are caused by time-varying magnetic fields, fields that depend on the orientation of the aircraft etc. Soft-iron errors are very difficult to compensate due to their time-varying nature. S_{sf} is the matrix containing scale factors for applied fields along the sensitive axis and off axes. $\delta\vec{B}_b$ is the vector of biases introduced due to hard-iron effects. Hard-iron errors are caused due to permanent magnetic fields that are fixed with respect to the sensor. These sources introduce a fixed offset in the magnetic sensor measures and can be compensated. Figure 3.12 shows x and y-axis readings collected from a solid state magnetometer with and without distortion. A piece of ferrous metal is placed close to the sensor to introduce the distortion. It can be seen that the center of ellipse containing the x and y readings is offset, in the presence of distortion.

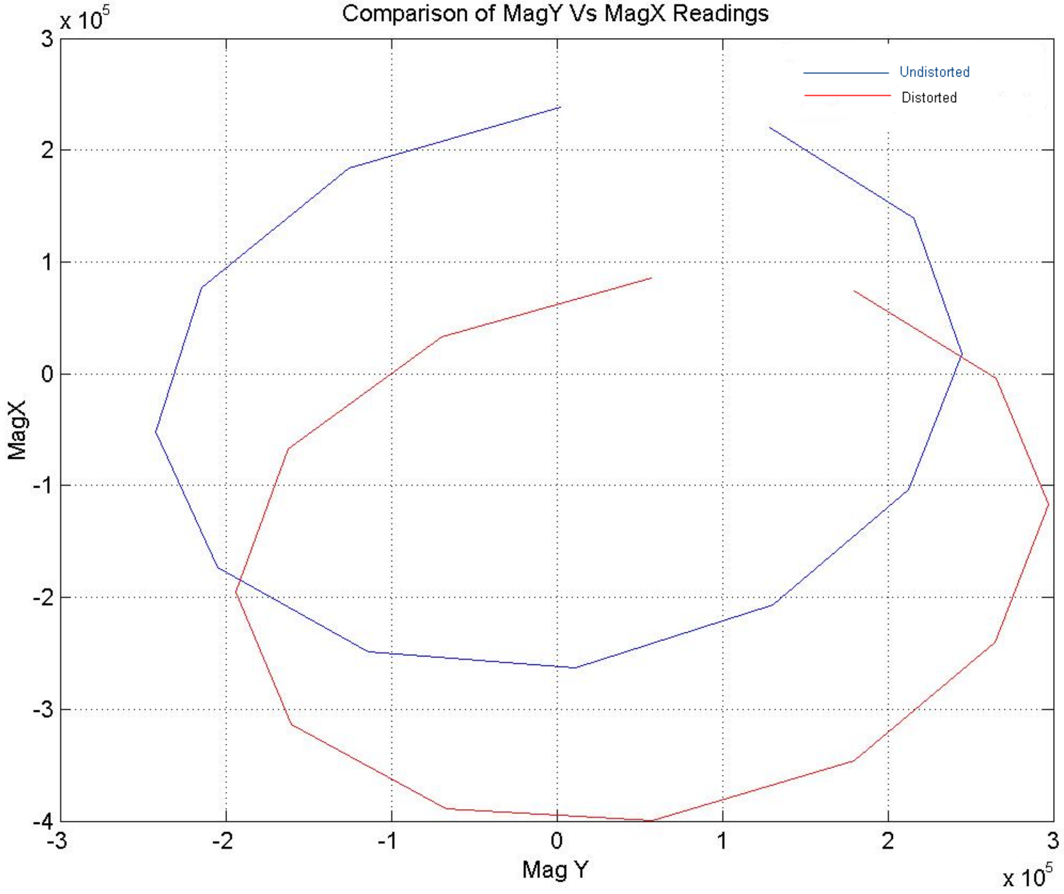

Figure 3.12: Hard Iron Effect

In this work, the general magnetometer model is simplified to assume that the soft-iron errors are minimized by the installation. Calibration methods are described to estimate the hard-iron biases and the scale factor matrix.

3.5.2 Magnetometer Calibration

Calibration of a magnetic sensor involves the determination of the scale factor matrix and the hard-iron offsets. If the magnetic sensor is mounted at a different location than the primary attitude sensors, an additional rotation matrix will also need to be determined. In this work, it is assumed that the magnetic sensor frame and the attitude sensor frames coincide. Also, it is assumed that the soft-iron errors are negligible and the magnetic sensor can be leveled or a means is available to determine the inclination of the magnetic sensor with respect to the local level. The measurement equation can be rewritten as:

$$\begin{bmatrix} B_x \\ B_y \\ B_z \end{bmatrix} = \begin{bmatrix} S_{xx} & S_{xy} & S_{xz} \\ S_{yx} & S_{yy} & S_{yz} \\ S_{zx} & S_{zy} & S_{zz} \end{bmatrix} \begin{bmatrix} c_{11} & c_{12} & c_{13} \\ c_{21} & c_{22} & c_{23} \\ c_{31} & c_{32} & c_{33} \end{bmatrix} \begin{bmatrix} H_x \\ H_y \\ H_z \end{bmatrix} + \begin{bmatrix} \delta B_x \\ \delta B_y \\ \delta B_z \end{bmatrix} \tag{3.20}$$

Assuming that the rotation matrix ${C_i}^b$ is known, applying an input magnetic field along the z-axis in the positive and negative direction gives the set of equations:

$$\begin{bmatrix} B_{x1} \\ B_{y1} \\ B_{z1} \end{bmatrix} = \begin{bmatrix} S_{xz}H_z \\ S_{yz}H_z \\ S_{zz}H_z \end{bmatrix} + \begin{bmatrix} \delta B_x \\ \delta B_y \\ \delta B_z \end{bmatrix} \tag{3.21}$$

and

$$\begin{bmatrix} B_{x2} \\ B_{y2} \\ B_{z2} \end{bmatrix} = \begin{bmatrix} -S_{xz}H_z \\ -S_{yz}H_z \\ -S_{zz}H_z \end{bmatrix} + \begin{bmatrix} \delta B_x \\ \delta B_y \\ \delta B_z \end{bmatrix} \tag{3.22}$$

where H_z is the applied field along the z-axis of the sensor. The scale factor column vector $\left[S_{xz}S_{yz}S_{zz}\right]^T$ can be determined from the above equations. The rest of the scale factor matrix can be determined in a similar fashion, but the installation magnetic environment is very likely to alter the scale factors. It is best to estimate the remaining elements of the scale factor matrix and the hard-iron biases through a compass swing calibration method, with the sensor mounted on the aircraft. A compass swing procedure involves rotating the aircraft through a circle to collect readings along reference heading directions as shown in Figure 3.13 [17].

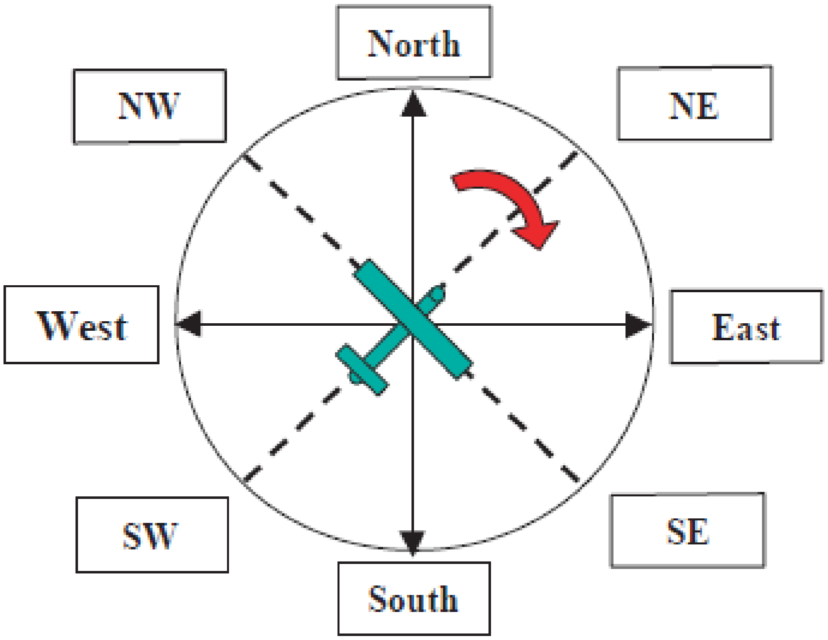

Figure 3.13: Compass Swing

Readings are collected and averaged with the aircraft stationary at each reference heading and post-processed to extract the hard-iron biases and the scale factor terms. With the latitude and longitude information, the horizontal and vertical components of the Earth's field at the geographic location can be determined with standard magnetic models such as WMM or IGRF. Given the inclination at each compass swing calibration point, the components of the Earth's magnetic field in the body fixed frame can be determined using the equations:

$$\begin{bmatrix} Hx_b \\ Hy_b \\ Hz_b \end{bmatrix} = \begin{bmatrix} \cos\theta & 0 & -sin\theta \\ \sin\phi\sin\theta & \cos\phi & \sin\phi\cos\theta \\ \cos\phi\sin\theta & -\sin\phi & \cos\phi\cos\theta \end{bmatrix} \begin{bmatrix} H_x \\ H_y \\ H_z \end{bmatrix} \tag{3.23}$$

If N is the number of calibration points around the circle, this leads to a set of N linear equations in x,y and z:

$$\begin{bmatrix} Hx_b & Hy_b & 1 \\ \vdots & \vdots & \vdots \end{bmatrix} \begin{bmatrix} S_{xx} \\ S_{xy} \\ \delta B_x \end{bmatrix} = \begin{bmatrix} \hat{B}_{x1} - S_{xz} \times Hz_b \\ \hat{B}_{x2} - S_{xz} \times Hz_b \\ \vdots \end{bmatrix} \tag{3.24}$$

$$\begin{bmatrix} Hx_b & Hy_b & 1 \\ \vdots & \vdots & \vdots \end{bmatrix} \begin{bmatrix} S_{yx} \\ S_{yy} \\ \delta B_y \end{bmatrix} = \begin{bmatrix} \hat{B}_{y1} - S_{yz} \times Hz_b \\ \hat{B}_{y2} - S_{yz} \times Hz_b \\ \vdots \end{bmatrix} \tag{3.25}$$

$$\begin{bmatrix} Hx_b & Hy_b & 1 \\ \vdots & \vdots & \vdots \end{bmatrix} \begin{bmatrix} S_{zx} \\ S_{zy} \\ \delta B_z \end{bmatrix} = \begin{bmatrix} \hat{B}_{z1} - S_{zz} \times Hz_b \\ \hat{B}_{z2} - S_{zz} \times Hz_b \\ \vdots \end{bmatrix} \tag{3.26}$$

The above equations are solved using least-squares to determine S_{xx}, S_{xy}, S_{yx}, S_{yy} and the hard-iron biases δB_x,δB_y and δB_z. Figure 3.14 below shows the post-calibration heading error in degrees at each compass swing point. The distorted data set generated to demonstrate hard-iron biases is post-processed to generate these results.

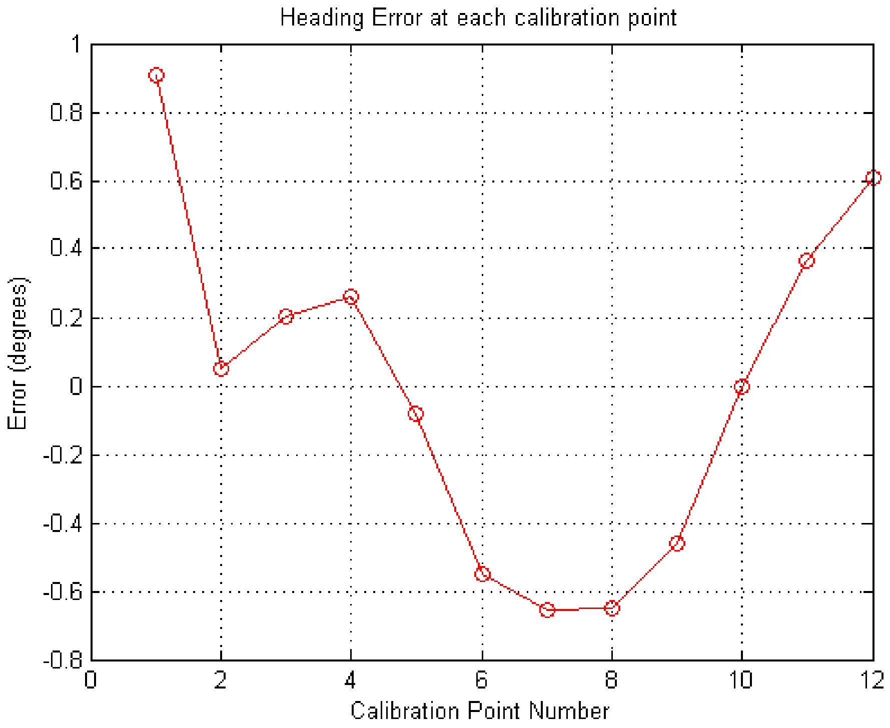

Figure 3.14: Heading Error Post-Calibration

The post calibration heading error shown above represents the best-case scenario under a benign environment. Actual compass calibrations on aircraft using this method have shown heading errors of less than 2 degrees.

Chapter 4

Attitude Estimation Algorithm Formulation

4.1 Introduction

This chapter describes the proposed algorithm using rotational quaternions to estimate 3-DOF attitude using low cost MEMS gyros, accelerometers and magnetometers. The attitude estimation algorithm proposed in this chapter is based on the quaternion formulation of SO(3) complementary filtering [12] reviewed in Chapter 2. The algorithm combines the quaternion formulation with fuzzy logic concepts to build a stable attitude estimation system. The motivation for the modification to [12] is given followed by the formulation of the proposed algorithm. Model parameters for gyros and accelerometers determined in the previous chapter are used in the development of the algorithm to select the fuzzy controller parameters.

In formulating the attitude estimation algorithm, the following assumptions are made:

- Measurements from a triad of MEMS gyros, accelerometers and magnetometers are available.
- MEMS gyroscope outputs are calibrated to minimize scale factor and misalignment errors.
- MEMS accelerometer outputs are calibrated to minimize scale factor and misalignment errors.
- Magnetometer is calibrated using the compass swing procedure described earlier to minimize hard-iron and scale factor errors. Soft-iron errors are assumed to be negligible.

- Startup alignment time of 2 minutes to capture the random turn-on bias of the MEMS gyros. The residual bias in the gyros are corrected by augmentation with accelerometers and magnetometers.

4.2 Motivation

Estimates of Euler roll and pitch angles can be computed from the x and y-axis accelerometer measurements as:

$$\theta_r = \sin^{-1}(A_x) \tag{4.1}$$

$$\phi_r = \sin^{-1}\left(\frac{-A_y}{\cos\theta}\right) \tag{4.2}$$

where θ_r is the pitch angle, ϕ_r is the roll angle, A_x represents the component of gravitational acceleration measured along the x-axis of body frame and A_y is the component along the y-axis of body frame. The above equations for roll and pitch angle assume that the inertial acceleration of the aircraft (coordinatized in the body frame) is negligible. An estimate of the magnetic heading can be computed from the magnetometer measurements using the equations in Chapter 3. The Euler angle estimates derived from the accelerometers and magnetometer measurements constitute the 'reference' attitude in this work and in [12].

The nonlinear observer proposed in [12] provides good tracking performance with a known attitude matrix or a quaternion or when the Euler angle estimates from accelerometers and magnetometer provide true attitude information, albeit corrupted with high frequency noise. The estimated attitude from this constant gain observer tends to track the 'reference' attitude very well. The observer functions as a complementary filter by rejecting high frequency noise from accelerometers and magnetometers and low frequency bias from the gyroscopes. However, the observer shows large deviations in the estimated attitude during accelerated maneuvers.

To illustrate this, consider a takeoff record from flight data with forward linear acceleration shown in Figure 4.1. The plot shows the pitch angle estimate derived from the x-axis accelerometer and the true pitch angle during the maneuver.

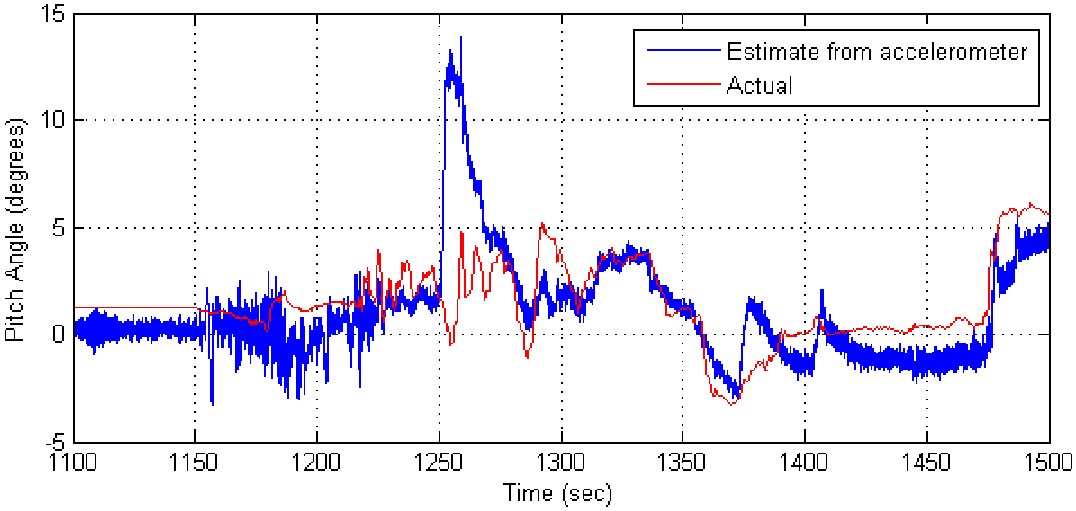

Figure 4.1: Take-off Maneuver

The effect of forward acceleration is to produce a pitch angle estimate (θ_r), that is significantly different from the true pitch attitude. If θ_r is used in the observer to derive the error quaternion components $\tilde{s}, \tilde{v}$ and correct the angular rate measures, the estimated attitude output will exhibit large deviations from the true attitude. To demonstrate a similar problem in estimating roll attitude, the following maneuvers are simulated and the estimated roll angles are compared with the true roll angle:

- Sinusoidal platform roll motion where the y-axis accelerometer provides a good 'reference' estimate of roll attitude.

- Coordinated turn (or steady banked turn) where the side force along the y-axis of body frame is zero and hence the y-axis accelerometer reading is essentially null. The accelerometer reading gives no useful measure of the true roll attitude.

Shown in Figure 4.2 is the roll estimate from a 15° sinusoidal platform motion - the estimated attitude tracks the true attitude quite well. In this case the measurement unit is subjected only to gravitational acceleration and the y-accelerometer provides useful information about the bank angle.

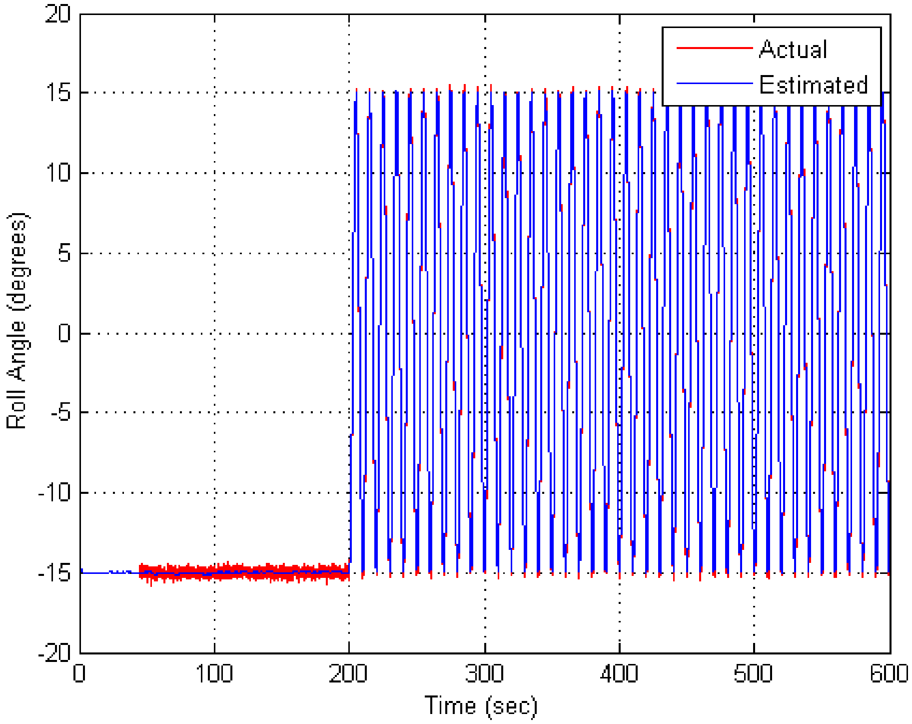

Figure 4.2: Sinusoidal Motion Roll Angle - Constant Gain

In a coordinated turn, the constant-gain estimator incorrectly applies a rate correction based on the attitude quaternion error. Figure 4.3 shows a simulation of this condition where a roll rate input of 23 deg/sec is applied but the roll estimate from the y-axis accelerometer is close to zero, as a result of the no-slip, banked turn.

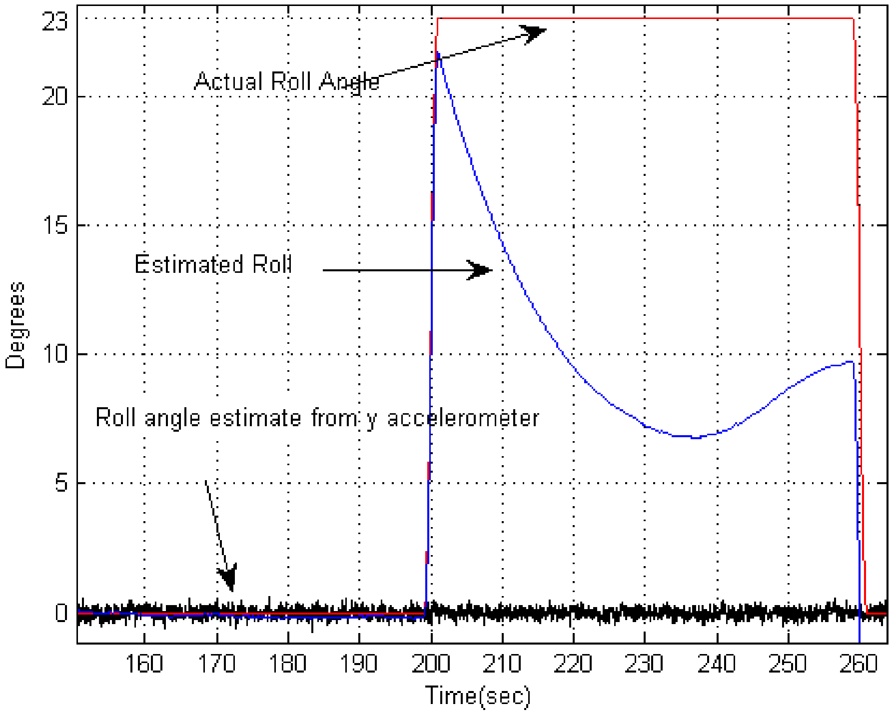

Figure 4.3: Coordinated Turn Roll Angle - Constant Gain

In this case a large deviation is observed between the true and the estimated roll angles. It can be concluded from the above simulations that a constant gain estimator tracks the reference attitude quaternion very well, but does not prevent a corrupted reference measurement from propagating to the quaternion estimate. Therefore, an independent attitude measurement is required in the estimators proposed in [12] and [18] to provide accurate attitude and bias estimates. This result is similar to a Kalman filter that is updated with corrupted measurements.

4.3 Proposed algorithm

To alleviate the problem of a 'corrupted measurement' propagating to the quaternion estimate, it is proposed that the nonlinear observer be modified to generate the estimator gains by using a fuzzy controller. A block diagram representation of the proposed algorithm is shown in Figure 4.4.

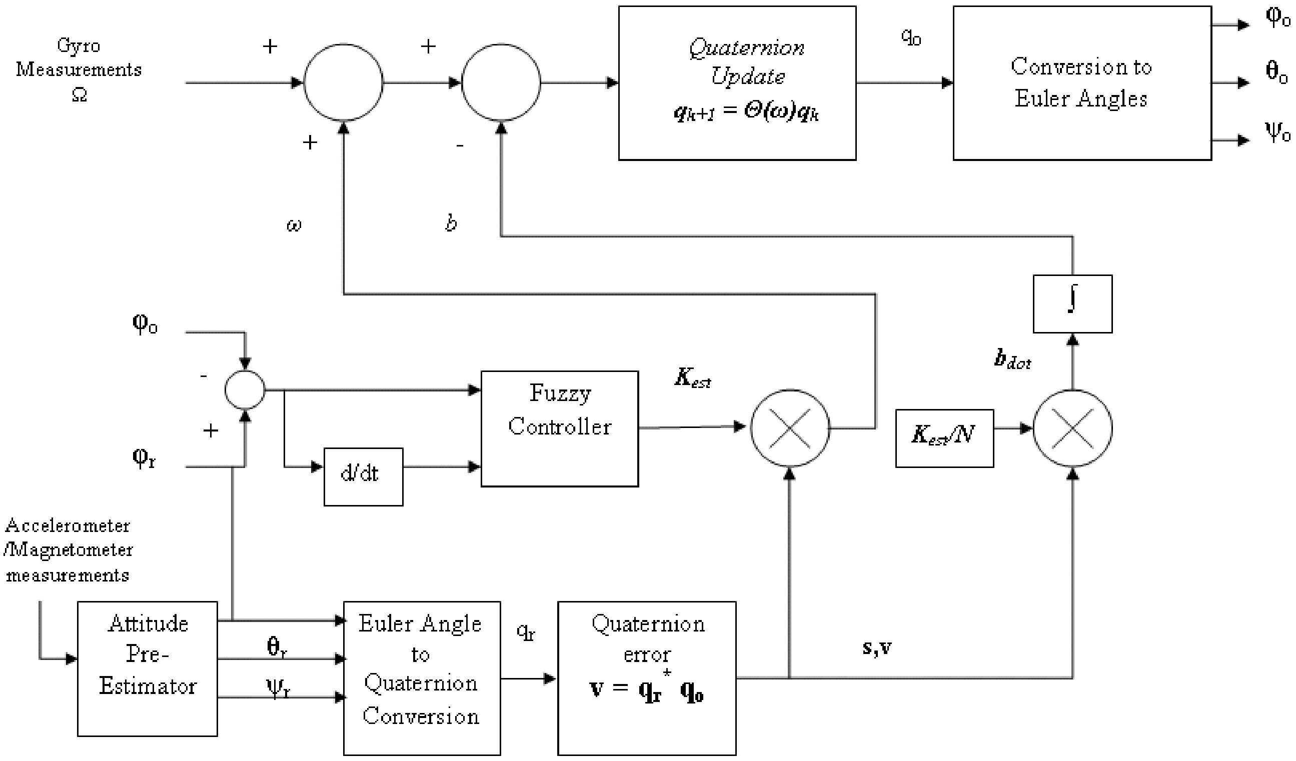

Figure 4.4: Proposed Attitude Estimator

The angular rates from the gyros are given by Ω. The attitude pre-estimator generates the 'reference' Euler angle estimated - ϕ_r, θ_r and ψ_r, from the accelerometers and magnetometer measurements. The 'reference' attitude is converted to a 'reference' quaternion q_r before generating the quaternion error. The estimator gain K_{est}, instead of a constant value, is now generated by a fuzzy controller. The fuzzy controller monitors the residual between the 'reference' attitude derived from the attitude pre-estimator and the estimated (output) attitude, and the rate of change of the residual to adaptively adjust the estimator gains K_{est}. Using this approach, it is theorized that the effect of transients or false information in 'reference' attitude on the estimates can be minimized. The block diagram shows only the roll angle ‘error’ and ‘rate of error’ inputs to the fuzzy controller. A similar controller is implemented for pitch attitude using the pitch angle ‘error’ and ‘rate of error’. To demonstrate the behavior of the fuzzy - non linear estimator the sinusoidal motion and the coordinated turn simulations in the previous sub-section are revisited in Chapter 5. The formulation of the attitude estimation equations is given below:

The quaternion observer kinematics proposed by [12] is restated here for completeness:

$$\dot{\hat{q}} = \frac{1}{2}\hat{q} \otimes p(\Omega - \hat{b} + \omega) \tag{4.3}$$

with

$$\dot{\hat{b}} = -k_b \tilde{s}\tilde{v} \tag{4.4}$$

and

$$\omega = k_{est}\tilde{s}\tilde{v} \tag{4.5}$$

where Ω is the measured angular rate, $\hat{b}$ is the estimated bias and ω is the angular rate correction. For the proposed algorithm, these equations can be rewritten as

$$\dot{\hat{q}} = \frac{1}{2}\hat{q} \otimes p(\Omega - \hat{b} + \omega) \tag{4.6}$$

with

$$\omega = k_{est}(t)\mathrm{sgn}(\tilde{s})\tilde{v} \tag{4.7}$$

and

$$\dot{\hat{b}} = -k_b(t)\mathrm{sgn}(\tilde{s})\tilde{v} \tag{4.8}$$

where $\hat{b}$ is the bias estimate that is initialized with the bias estimates from alignment and $k_{est}(t)$ and $k_b(t)$ are time-dependent values generated by a fuzzy controller.

Trapezoidal integration method is used to integrate and estimate q_{k+1} from the corrected body rates, and the components of the updated attitude quaternion are renormalized to maintain a unity norm.

$$q_{k+1} = q_k + \frac{T}{4}\big(Q_k\Delta_k + Q_{k-1}\Delta_{k-1}\big) \tag{4.9}$$

with $\Delta_k = \Omega - \hat{b} + \omega$ and Q_k is the 4x4 matrix given by

$$Q_k = \begin{bmatrix} q_0 & -q_1 & -q_2 & -q_3 \\ q_1 & q_0 & -q_3 & q_2 \\ q_2 & q_3 & q_0 & -q_1 \\ q_3 & -q_2 & q_1 & q_0 \end{bmatrix} \tag{4.10}$$

The estimated attitude quaternion q_{k+1} at each integration step is converted to Euler angles for output. The rate and bias correction equations can be viewed as the proportional and integral paths of a correction loop for attitude and bias errors. Since the vector part of the attitude quaternion is analogous to a rotation axis, the rate correction terms ω_x, ω_y and ω_z derived from the quaternion error can be viewed as corrections to the angular velocity vector and allow the estimated quaternion to track the reference quaternion dynamics. The bias estimate terms $\hat{b}_x$, $\hat{b}_y$ and $\hat{b}_z$ track the gyro bias under quiescent conditions. The angular rate corrections for x, y and z-axis gyros are updated using the equations:

$$\omega_x = k_x(t)\mathrm{sgn}(\tilde{s})\tilde{v_x} \tag{4.11}$$

$$\omega_y = k_y(t)\mathrm{sgn}(\tilde{s})\tilde{v_y} \tag{4.12}$$

$$\omega_z = k_z(t)\mathrm{sgn}(\tilde{s})\tilde{v_z} \tag{4.13}$$

Following the exponentially correlated bias model in [14], the modified bias estimate update equations can be written as:

$$\dot{\hat{b}} = \frac{-1}{\tau}\hat{b} + \frac{k_{est}}{N}\tilde{s}\tilde{v} \tag{4.14}$$

where N is a scaling constant and τ is the time constant of the first-order Gauss Markov process. The gain k_b is chosen as a scaled version of k_{est} to sufficiently decouple the bias update equations from attitude errors. Also, under dynamic conditions, the fuzzy controller lowers the estimator gain k_{est} and choosing

$$k_b = \frac{k_{est}}{N} \tag{4.15}$$

ensures that the bias update equation preserves the last bias estimate. The time constant τ of the exponentially correlated bias model was determined from experimental autocorrelation data to be 500 seconds. Since $\tau >> 1$ sec, a first order approximation of the bias update equation gives

$$\hat{b}_{k+1} = \hat{b}_k + T_s \frac{k_{est}}{N} \tilde{s}\tilde{v} \tag{4.16}$$

Since the gyro biases are slowly varying, the bias estimation gain k_b is picked to be 100 times smaller than $k_e st$. For a constant gyro bias, convergence to the true bias is assured [12] if

$$k_b > \frac{2\tilde{b}(0)}{2 - E(0)} \tag{4.17}$$

where E(0) is the initial value of the cost function and $\tilde{b}(0)$ is the initial bias error. In this case, the alignment step produces an initial estimate of gyro bias by averaging the rate sensor readings and hence $\tilde{b}(0)$ is small - a typical value being 0.01 deg/sec. Also, if the accelerometer bias is negligible, the initial quaternion estimate is assumed to be equal to the 'reference' quaternion - the body and reference frames are coincident, and the initial cost function is zero.

To verify that the bias estimator tracks the gyro bias drift with these gain settings, static gyro readings are generated with a random turn-on bias, first order Gauss Markov source and white noise with the characteristics determined from sensor models in Chapter

3. Figure 4.5 shows the injected bias - sum of the exponentially correlated noise and turn-on bias, and the estimated bias for x,y and z-axis gyros.

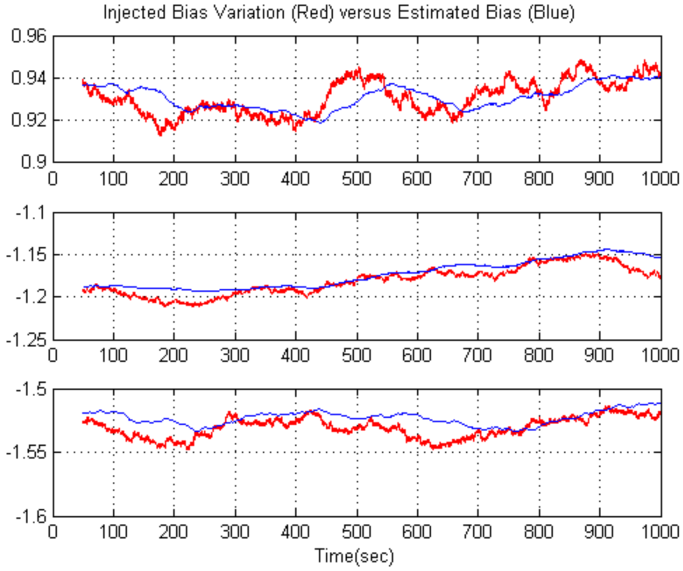

Figure 4.5: Injected and Estimated Gyro Bias

4.4 Fuzzy Controller Parameters

The model parameters determined in Chapter 3 are used in this section to select the fuzzy controller centers, widths and peak gains. The model parameters are restated here for completeness:

- Gyro Angular Random Walk of 2.1 deg/$\sqrt{hr}$.
- Gyro Bias Stability of 28 deg/hr.
- Gauss Markov variance of $3 \times 10^{-4} \left[deg/sec\right]^2$.
- Gauss Markov time constant of 500 sec.
- Accelerometer Bias Stability of 0.158 mg.

To generate the estimator gains $k_x(t), k_y(t)$, individual fuzzy controllers are used for roll and pitch estimation. The inputs to the fuzzy controllers are chosen as the difference between the Euler angle estimates computed from the accelerometers and the output Euler angles (the 'error' input or residual) and the rate of change of this residual. The reference magnetic heading computed from the magnetic sensor is assumed to be accurate, albeit noisy, and the gain derived from roll channel is used in place of k_z. To select the estimator gain k_{est} under quiescent conditions, and the widths of the 'zero' error input rules for roll and pitch the following argument is made:

If a white noise sequence is integrated for a time t, the variance of the output (exhibiting 'random walk') after time t is given by

$$V = \sigma^2 \times \delta t \times t \tag{4.18}$$

where δt is the sampling time, t is the integration time and σ^2 is the variance of the white sequence. Therefore, the standard deviation of the attitude error resulting from white noise in the gyro increases with $\sqrt{\delta t \times t}$. If the bias stability is modeled as a random walk for short periods of time, the attitude error contribution is a second order random walk that increases with $t^{\frac{3}{2}}$. For an unaided gyro output, given the model parameters above, the root sum square of the two errors results in an estimation error of about 1° (in roll angle) after a 60-second coordinated turn. Other factors that will increase this error are rate scale factor errors, misalignment errors and any bias errors entering the turn. Therefore, a conservative value of 2° error after 60 seconds is picked as the potential estimation error in attitude after the completion of the turn. The 'zero' error membership function width is chosen to be ±2° to allow the output attitude to converge quickly to the reference attitude. The 'zero' rate of error membership function width is chosen to be $\pm 1°/sec$. To select the gain k_{est} under quiescent conditions ('zero error' and 'zero rate of error'), an estimation error of 4 degrees in roll angle is artificially introduced with the true roll attitude set to zero as shown in Figure 4.6.

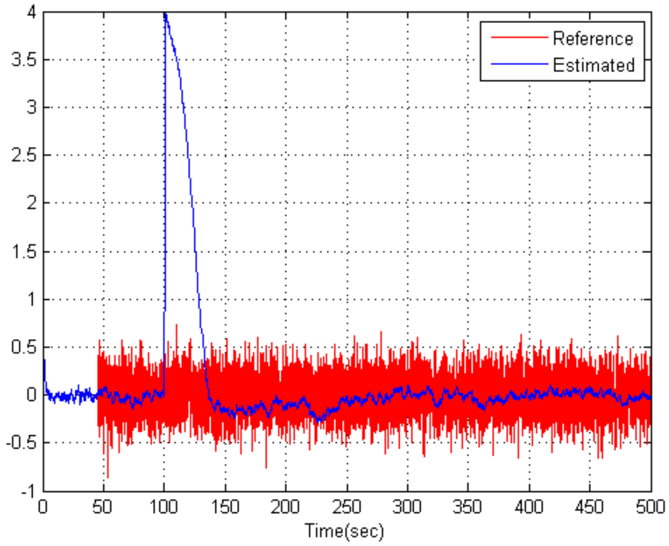

Figure 4.6: Roll Angle Convergence

The maximum gain k_{est} is set to 0.5 rad/sec to get a time constant of approximately 20 seconds. Since $k_{est} > 0$, the stability of the estimator for this gain setting follows from [12].

With the center and widths of the 'zero error' and 'zero rate of error' picked, the centers and widths of 'negative small', 'positive small', 'negative medium' etc., are picked to be equally spaced with identical widths. The output gains corresponding to these membership functions are picked to decrease by a factor of 2, as the 'error' or 'rate of error' increases. The gain profiles used by the fuzzy controller for roll and pitch channels are shown in Figures 4.7 and 4.8.

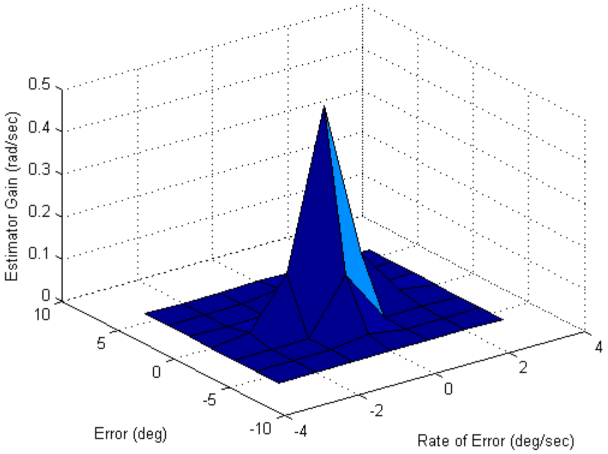

Figure 4.7: Gain Profile for Roll Attitude

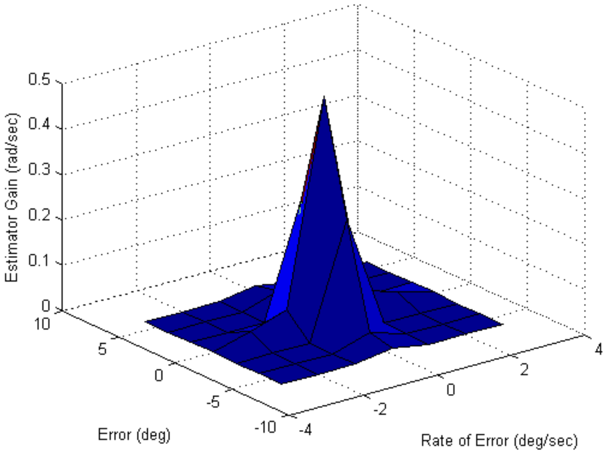

Figure 4.8: Gain Profile for Pitch Attitude

The surface plots represent the possible fuzzy controller outputs as a function of the 'error' and 'rate of error' inputs. The surface is shaped by the overlap of the centers and widths of the triangular membership functions used in this work. The surface represents an interpolation between the mappings described by the membership functions. To provide finer tuning, seven membership functions are used to define rules for 'zero', 'small', 'medium and ‘large’ positive and negative error. Similarly, seven membership functions are used for the rate of error input. The centers and widths of the input rules are picked to be symmetric on either side of the ’zero’ rule. Thus, the ‘negative small’ error rule is centered at $-2°$, the ‘negative medium’ rule is centered at $-4°$ etc. Under level flight conditions, when the error e and the rate of change of error $\dot{e}$ are ‘zero’, the output attitude quaternion converges to the reference quaternion q_r and the output Euler angle estimates converge to the reference angles. Under dynamic flight conditions, as the error e or $\dot{e}$ increases, the rate correction and the bias integration gains are lowered by the fuzzy controller so that transients in q_r can be rejected.

Chapter 5

Performance Studies

5.1 Overview

This chapter presents a description of simulation studies and the results obtained using the proposed attitude estimation algorithm to demonstrate compliance with some of the requirements for an Attitude Heading Reference System. The sinusoidal motion and coordinated turn simulations from Chapter 4 are exercised to highlight the effect of introducing the fuzzy controller and to compare the results from the constant gain estimator. Real world flight test inputs from an inexpensive inertial measurement unit are used to assess the performance in flight and the results are compared with those from an aided Kalman filter algorithm and outputs from a reference attitude estimator. The robustness of the proposed algorithm is studied by evaluating the performance with no external aiding.

5.2 Simulation Studies

Depending on the operating modes that are supported, attitude heading reference systems are required to meet a minimum set of performace tests per various Technical Standard Orders (TSO). For example, a settling error of less than 2 degrees after one hour of sinusoidal motion is required to be compliant with TSOC4c Bank and Pitch Instruments[15]. If a directional gyro heading mode is supported, the system is required to meet TSOC5e Direction Instrument[16]. The simulation studies presented in this section were conducted to obtain results for a few of these standard tests and assess the performance of the proposed algorithm. The following tests are simulated by generating time series data in Simulink for body frame gyroscopic rates, accelerations and magnetic field components:

- Static Test
- Sinusoidal variation of body rates and accelerations
- Coordinated turn

The sensor models presented in Chapter 3 are used to corrupt the inputs with noise and bias. The gyroscopic outputs are corrupted with a random constant to simulate turn on bias, a first order Gauss-Markov process to simulate bias variation and white noise. Acceleration outputs are corrupted with white noise and the turn-on bias of the accelerometers is assumed to be negligible. The noise variance in magnetometer outputs is assumed to be negligible. The flight test studies use sensor outputs from an Archangel Systems,Inc. low cost inertial measurement unit (IM3) and a magnetic sensing unit (MSU). The parameters derived from the sensor models in Chapter 3 are used in the simulation studies.

The acceleration noise of the IM3 is less than 0.002 G but the simulation value is set to 0.01 G to account for any seismic noise. The result of a 500-second static simulation with inclinations -5 degree bank and the 2 deg elevation with a west heading is shown in Figure 5.1. The estimated attitude remains stable for the duration of the simulation. The convergence of the roll and pitch attitudes and the initialization of the heading after alignment can also be seen.

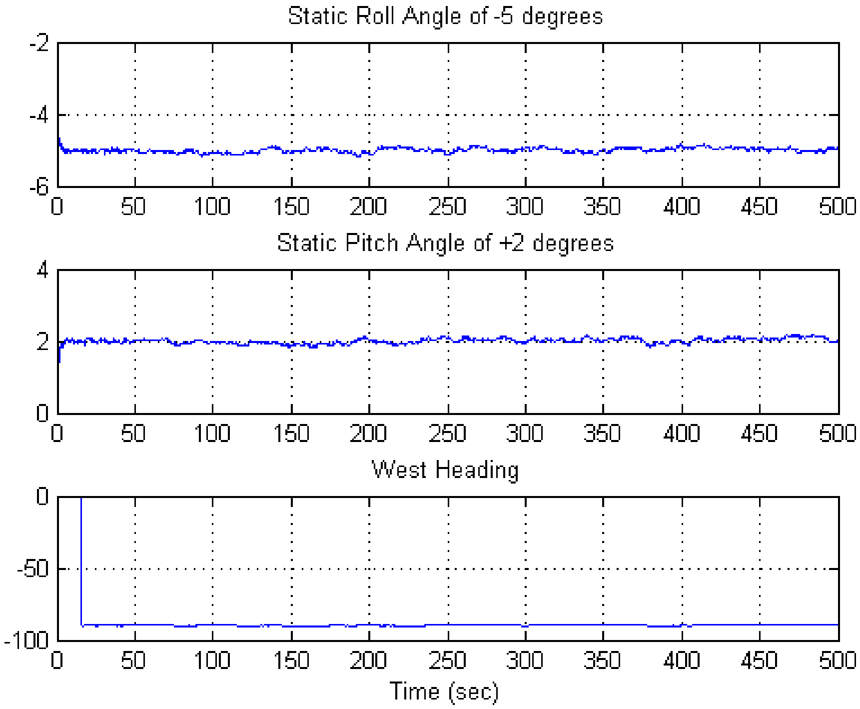

Figure 5.1: Static Simulation

The simulated sinusoidal platform motion is an angular motion with an amplitude of 15 degrees and a frequency of 0.1 Hz. The motion is imparted such that the roll and pitch motion are 90 degrees out-of-phase and the roll and yaw motion are in-phase. Figure 5.2 and Figure 5.3 show convergence of the estimated roll and pitch attitude to the static attitude after 3000 seconds of sinusoidal motion.

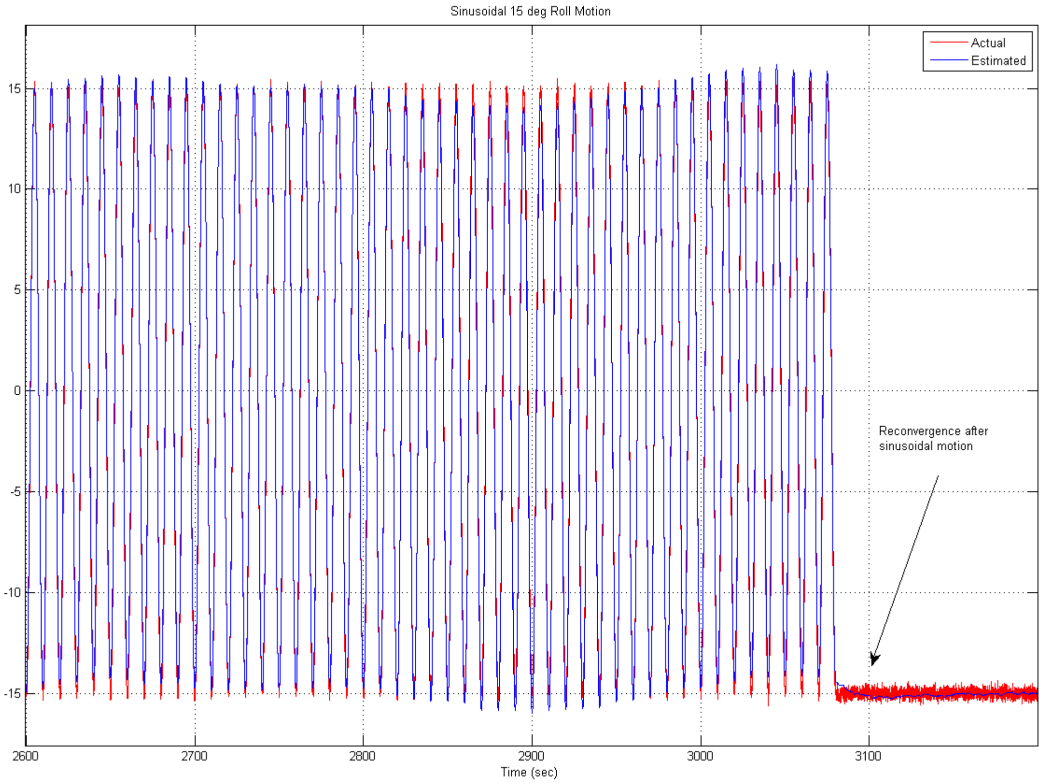

Figure 5.2: Sinusoidal Roll Motion

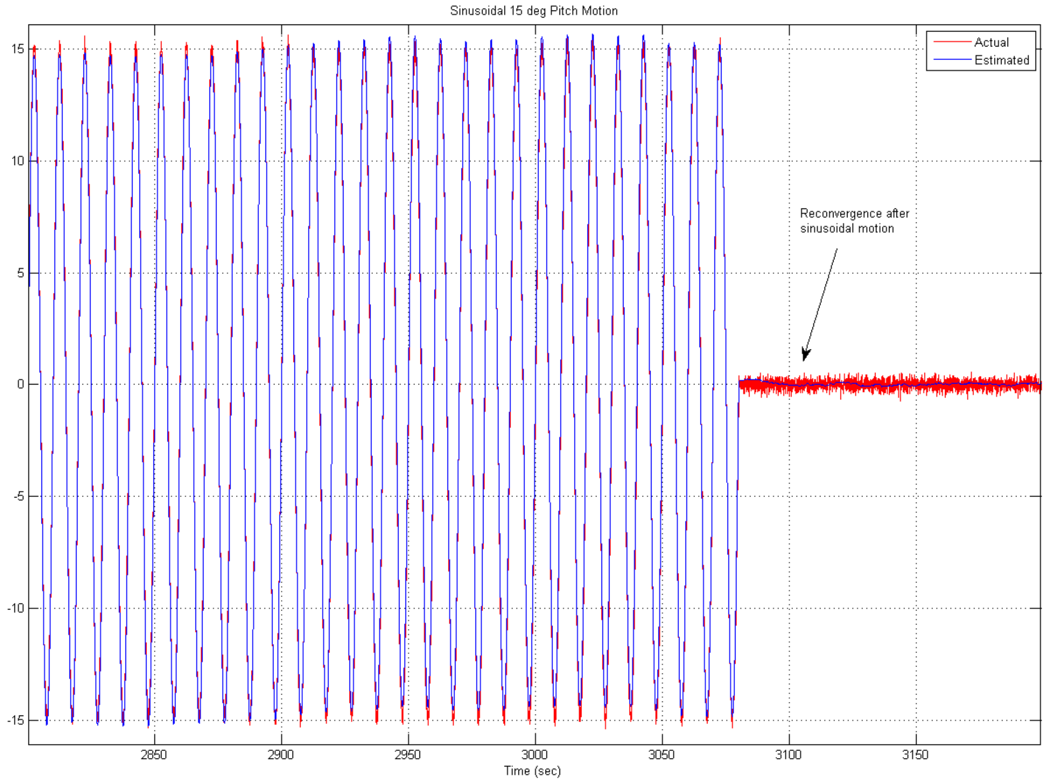

Figure 5.3: Sinusoidal Pitch Motion

A standard coordinated turn motion is simulated with a 3 degree/sec turn rate, 23 degree bank and 2 degree elevation. The coordinated motion results in a zero specific force on the y-axis accelerometer and no useful estimate can be generated. The estimated roll attitude for a left and right turn maneuvers are shown in Figure 5.4.

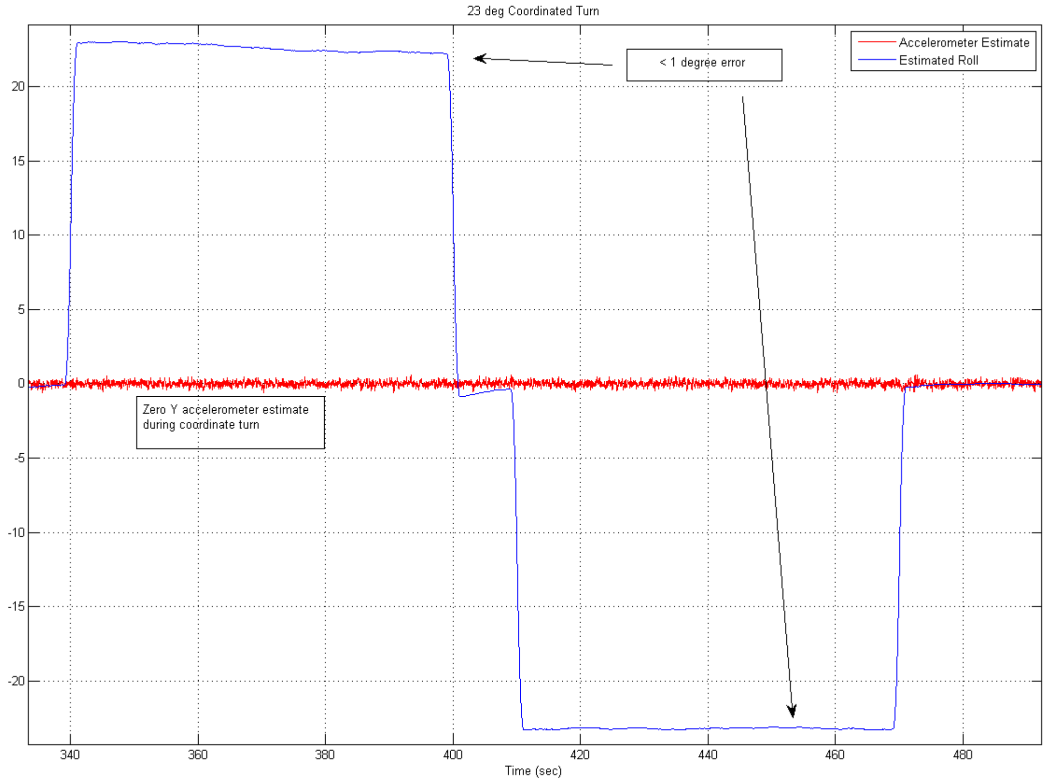

Figure 5.4: Roll Attitude During Coordinated Turn

The above simulation result can be compared with the constant gain estimator results in Figure 4.3. It can be seen that the effect of introducing the fuzzy controller is to decouple the false information from the Y accelerometer from the estimated quaternion. The deviation in the estimated roll at the end of the turn (t=400 sec) shows up as an undershoot and the roll attitude converges to the actual roll angle generated from the y accelerometer.

5.3 Flight Test Studies

In addition to the simulation studies, flight test performance studies of the proposed algorithm were conducted. For data collection a low cost inertial measurement unit (IM3) and a magnetic sensing unit (MSU) from Archangel Systems,Inc. were used. The sensor assembly is a part of a MEMS AHR150A Air Data Attitude Heading Reference System mounted on a Bell Helicopter tilt rotor aircraft. The gyroscopic rates and acceleration measurements are directly available from the recording stream. Also available in the recording stream are the attitude estimates from an onboard Honeywell ADAHRS, henceforth referred to as the ‘reference unit’. The reference ADAHRS is reported to be accurate within 2 degrees in roll and pitch attitude. The magnetic field components required to compute heading are generated by assuming a latitude/longitude and the attitude from the reference unit to transform the magnetic field measures to the body frame. The performance of the proposed algorithm is assessed under two conditions:

- Aiding with airspeed
- Loss of airspeed aiding

5.3.1 Performance with airspeed aiding

With airspeed aiding, the results from the proposed algorithm are compared with the attitude estimates from a Kalman filter estimator and the reference unit. The development of the Kalman filter state model and update equations is covered in Appendix A. Aiding with the airspeed input provides a better estimate of the gravity vector since the components of inertial acceleration (coordinatized in the body frame) can be removed from the specific force measurements. The results with airspeed aiding give an idea of the best case performance that can be achieved with the proposed algorithm. Flight data and results from the following high dynamic maneuvers (where an airspeed input is useful) are considered for comparison:

- Coordinated turn
- Takeoff Maneuver
- Approach to hover

Figure 5.5 shows the roll angle estimates generated by the proposed algorithm and the aided Kalman filter algorithm. The roll attitude recorded from the Honeywell ADAHRS reference unit is also shown. The deviations in the roll estimates between the three outputs are less than 2 degrees.

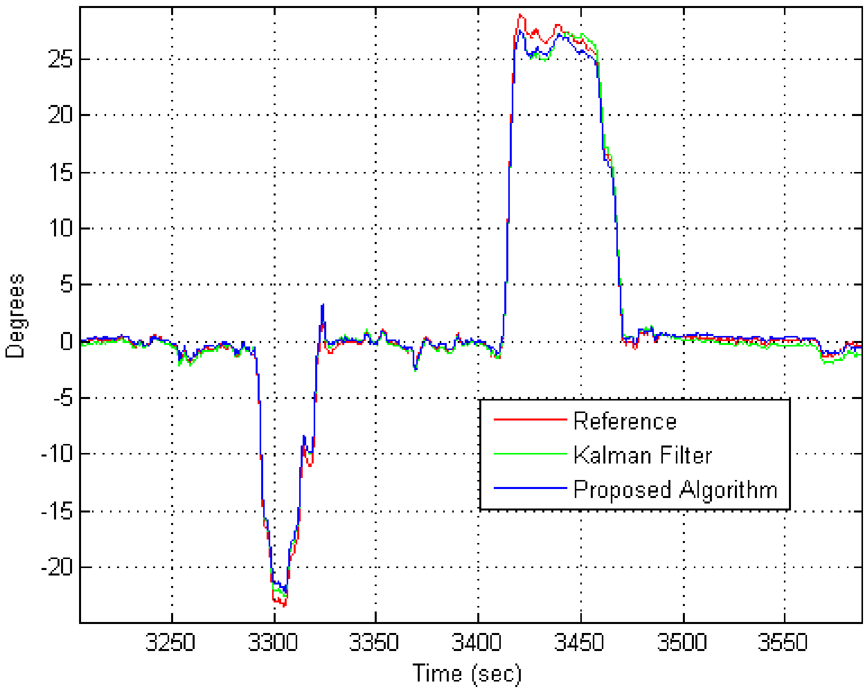

Figure 5.5: Aided Roll angle comparison between IKF and proposed algorithm

Figure 5.6 shows the pitch angle estimates during a takeoff maneuver with sustained linear acceleration. The estimate from the proposed algorithm tracks the pitch angle from the other two sources within 2 degrees.

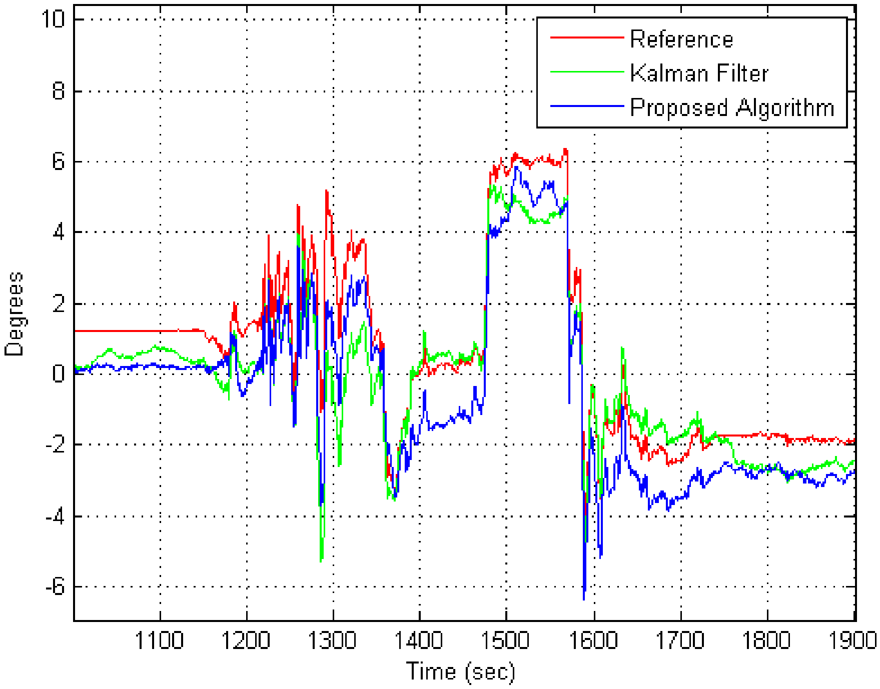

Figure 5.6: Takeoff pitch angle comparison between IKF and proposed algorithm

Figure 5.6 shows the roll and pitch estimates during an approach to hover maneuver with sustained deceleration. The attitude from the proposed algorithm tracks the other two sources within 2 degrees.

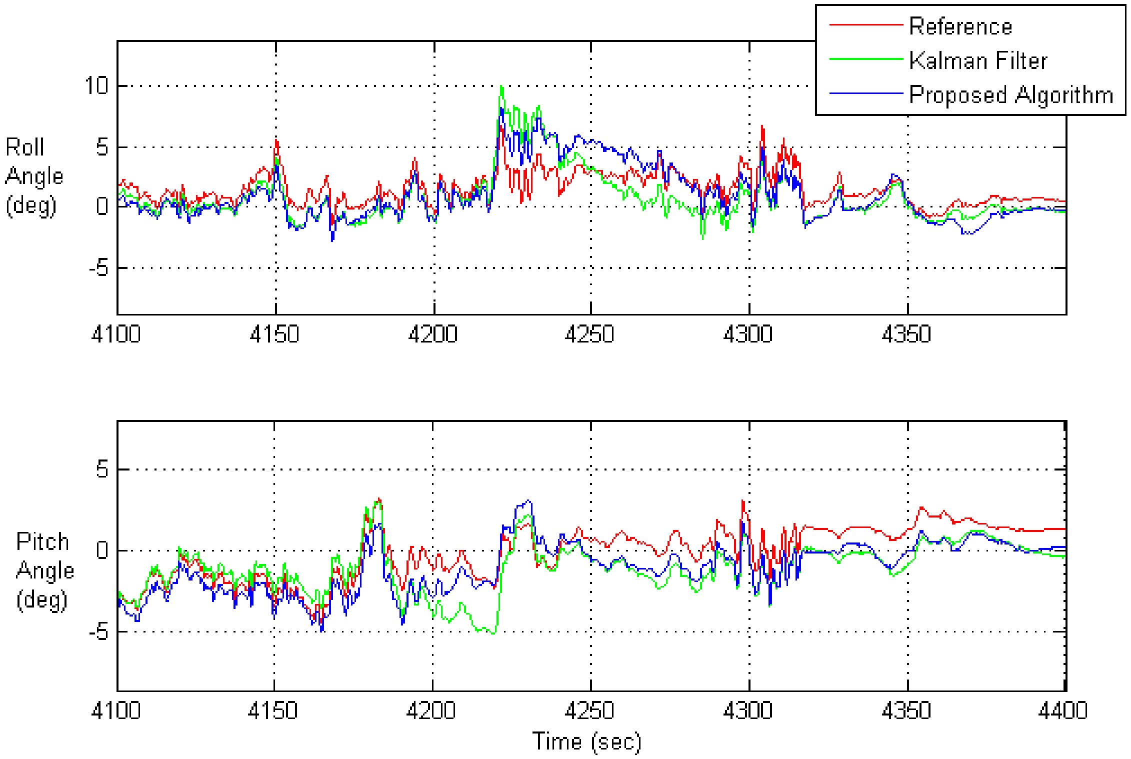

Figure 5.7: Approach to hover

The above results show that the non linear fuzzy algorithm performs well when airspeed aiding is available.

5.3.2 Performance under loss of aiding

To assess the robustness of the proposed algorithm under loss of aiding, the flight data is run through the proposed algorithm with no airspeed input and the results are compared with results from an Euler angle complementary filter algorithm used in the MEMS AHR150A. Figure 5.8 shows the estimated roll compared with the reference roll angle and the roll angle from the Euler angle baseline algorithm with no airspeed input. The plot also shows the deviations between the baseline and the proposed algorithms when compared with the output of the reference unit. The deviations in roll angle closely track the baseline algorithm with the peak deviation of approximately 4.3 degrees.

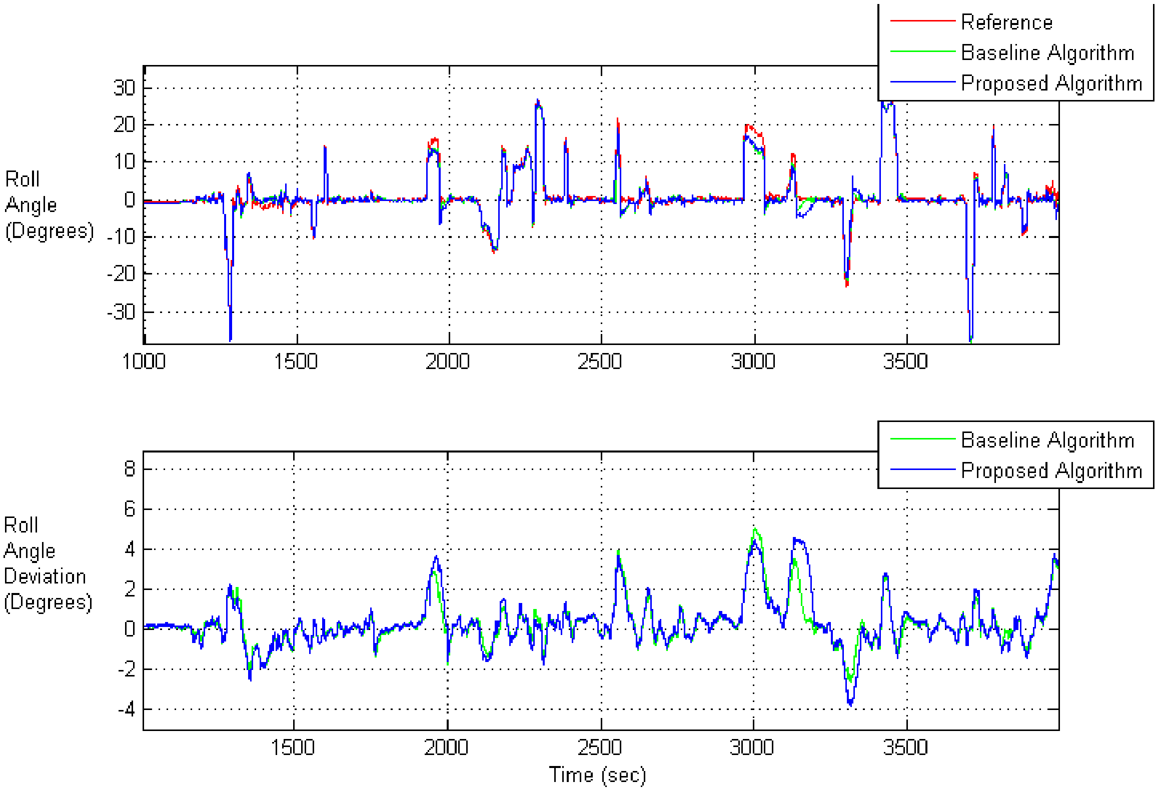

Figure 5.8: Unaided Roll Angle Comparison

Figure 5.9 shows the pitch angle comparison with the reference and the Euler angle baseline algorithm with no airspeed input. The plot also shows the deviations between the baseline and the proposed algorithms. The deviations in pitch angle match up well with the baseline results.

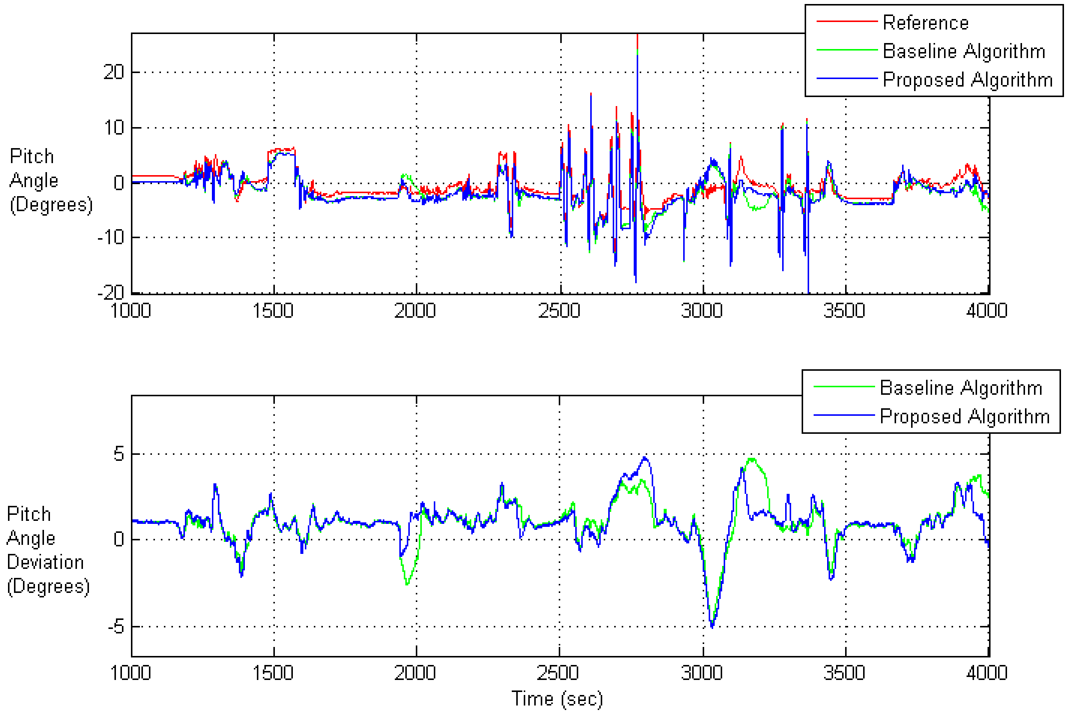

Figure 5.9: Unaided Pitch Angle Comparison

The maximum deviations in pitch are seen during the time period 2500-3500 seconds. The airspeed and x-axis acceleration profiles during this period (Figure 5.10) show a number of rapid acceleration and deceleration maneuvers, gradually reaching pitch attitudes close to 27°. Large discrepancies can be seen between the pitch angle estimate derived from x-axis accelerometer and the pitch angle from the reference unit. The maximum discrepancy between the two is approximately 27°. Airspeed aiding in such high dynamic maneuvers input is invaluable to achieve good attitude accuracy. Referring to Figure 5.9, it can be seen that the proposed algorithm is robust enough to provide a reasonable pitch attitude through the maneuver, although a buildup in pitch error could be observed.

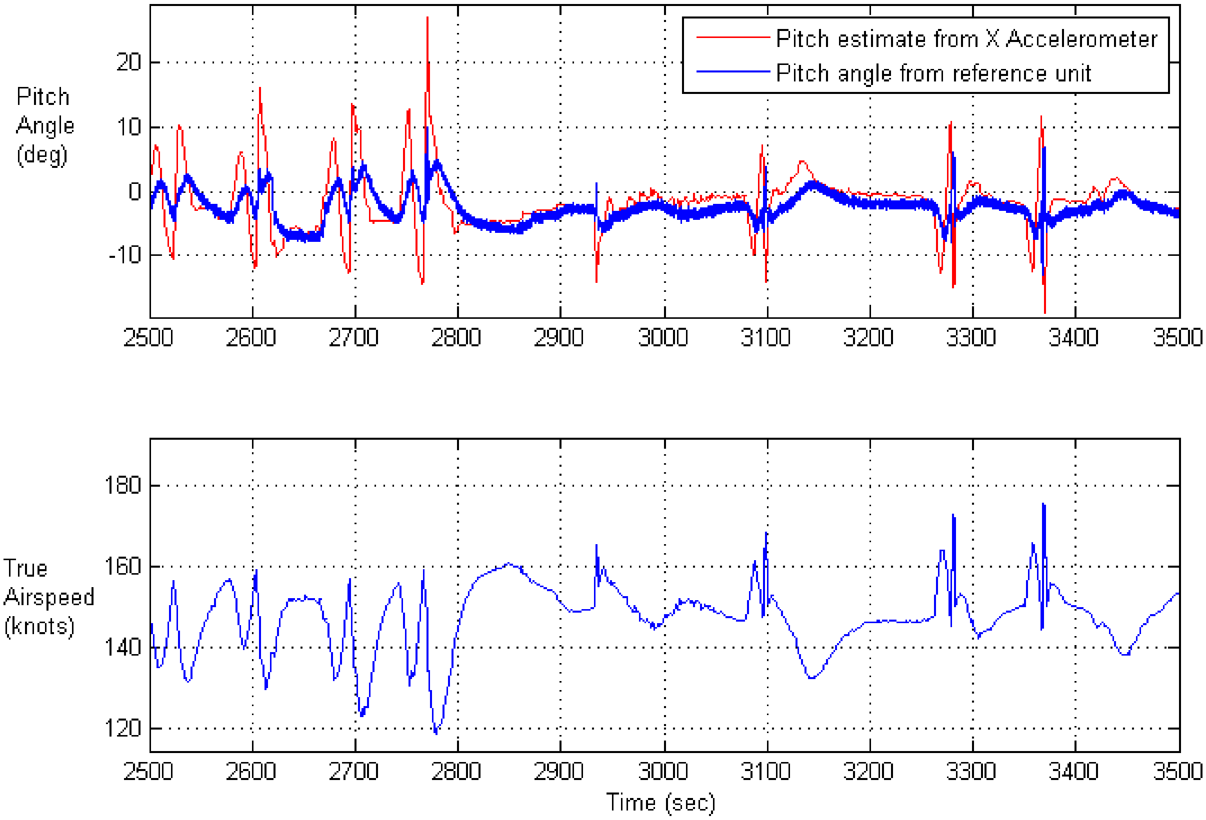

Figure 5.10: Pitch Estimate and Airspeed

The above results, in the absence of airspeed aiding, also show the effect of the introducing the fuzzy controller. Consider the takeoff record shown in Figure 5.11. The plot shows the pitch attitude from the onboard reference unit, the estimated pitch and the pitch reference obtained from the north accelerometer. Also shown are the inputs to the fuzzy controller - pitch attitude error and the rate of change of error, and the gain output of the controller. The pitch attitude from the onboard reference is assumed to be accurate. It can be seen that when the error input to the controller increases rapidly (t = 1250 sec), the controller reduces the output gain. When the error becomes "‘small"' (t = 1290 sec), the controller gain increases to the nominal "zero"' error value of 0.5 rad/sec.

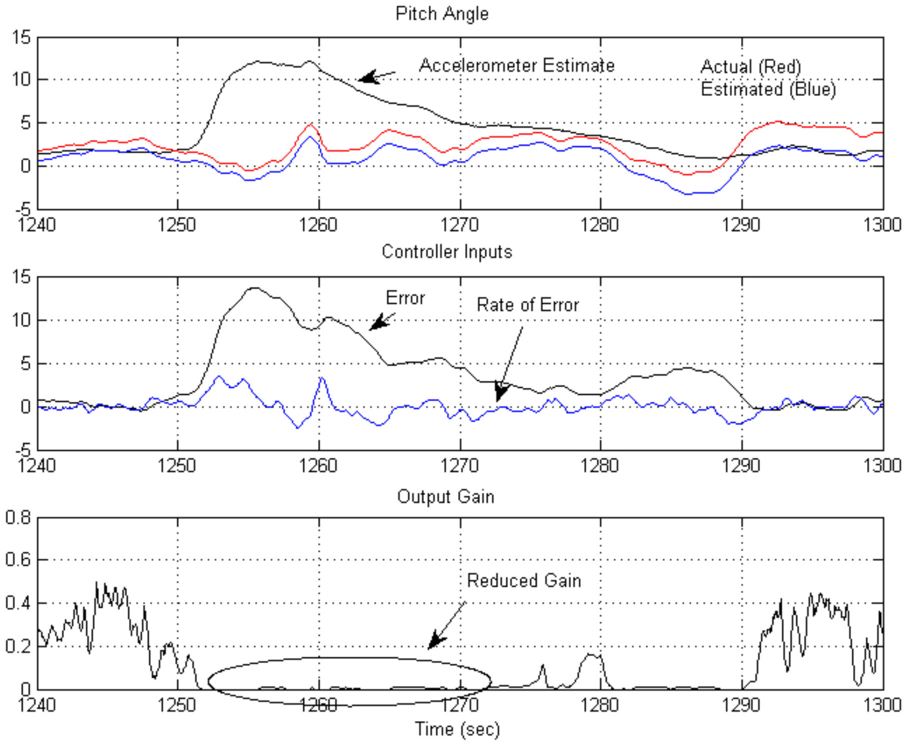

Figure 5.11: Takeoff Maneuver

The error statistics for the estimated roll and pitch attitude with the proposed algorithm are given in the table below. The errors are computed against the outputs of the reference unit.

Parameter	Unaided	Aided
Mean Roll(deg)	0.13	0.21
Std Roll(deg)	1.11	0.68
Mean Pitch(deg)	0.74	0.95
Std Pitch(deg)	1.31	0.56

Chapter 6

Conclusions

6.1 Overview

This dissertation presented a robust attitude estimation algorithm combining non linear observer techniques with an adaptive fuzzy logic controller for attitude and heading reference systems. The proposed estimation algorithm is an extension of the recent work on non linear attitude observers proposed by various authors for spacecraft applications. These observers, however, required an independent measurement of platform attitude to estimate the attitude error and the gyro bias and do not perform well when the augmentation sources provide false information. In the effort to address this problem, this dissertation reviewed some of the attitude representation and estimation techniques including non linear estimation techniques that operate in SO(3) and quaternion spaces. Sensors models for the low cost MEMS sensors used were presented and the model verification was performed by using techniques such as Allan Variance. Model parameters were used to develop the fuzzy logic-quaternion estimation algorithm that relies on gravity and magnetic vectors to derive the reference attitude. Flight test data were used to compare the estimation performance of the proposed algorithm with baseline results. In the presence of airspeed aiding, the algorithm was shown to provide attitude estimates comparable to other attitude estimators such as an extended Kalman filter. The robustness of the algorithm was shown by evaluating the performance from takeoff to landing with no external aiding sources like air data systems, GPS etc. The results of offline processing showed that, under loss of external aiding, the proposed algorithm performed reasonably well even through some dynamic maneuvers involving rapid accelerations. The overall performance of the proposed algorithm makes it ideal for implementation as part of an inexpensive backup attitude estimation system that can continue to provide attitude estimates when aiding sources are unavailable.

6.2 Future Work

Improving the estimation accuracy during high dynamic maneuvers, when no external aiding is available, is an obvious area for improvement in the adaptive correction scheme proposed in this work. Adding more fuzzy controller input rules could help in better predicting the conditions to engage and disengage augmentation. However, when the augmentation sources cannot be trusted, the bias stability of the gyro limits the achievable attitude accuracy and the growth of error. The proposed algorithm could be extended to fuse inputs from multiple aiding sources, for example GPS and an air data system, to provide attitude estimates and inertial velocity estimates for a hover-on-point application.

Bibliography

[1] IEEE Std 952-1997. IEEE standard specication format guide and test procedure for single-axis interferometric fiber optic gyros. *IEEE Standards Board*, 1997.

[2] D.W Allan. Statistics of atomic frequency standards. *Proceedings of the IEEE, Vol.54, No.2*, 1966.

[3] Albert-Jan Baerveldt and Robert Klang. A low-cost and low-weight attitude estimation system for an autonomous helicopter. *Intelligent Engineering Systems*, 1997.

[4] I.Y. Bar-Itzhack and M. Idan. Recursive attitude determination from vector observations: Euler angle estimation. *AIAA Journal of Guidance Control and Navigation*, 1987.

[5] I.Y. Bar-Itzhack and Y. Oshman. Attitude determination from vector observations: Quaternion estimation. *IEEE Transactions on Aerospace and Electronic Systems*, 1985.

[6] Neil Barbour and George Schmidt. Inertial sensor technology trends. *IEEE Sensors Journal*, 2001.

[7] Robert Grover Brown and Patrick Y.C. Hwang. *Introduction to Random Signals and Applied Kalman Filtering*. The American Institute of Aeronautics and Astronautics, 1997.

[8] C.Moler and G.Van Loan. Nineteen dubious ways to compute the exponential of a matrix. *SIAM review, Vol 20, No.4*, 1978.

[9] D.H.Titterton and J.L.Weston. *Strapdown Inertial Navigation Technology.* The American Institute of Aeronautics and Astronautics, 2004.

[10] Demoz Gebre-Egziabher et al. A gyro-free quaternion-based attitude determination system for implementation using low cost sensors. *Proceedings of the IEEE Position Location and Navigation Symposium*, 2000.

[11] R.C.Hayward et al. Inertially aided GPS based attitude heading reference system(ahrs) for general aviation aircraft. *Proceedings of ION-GPS*, 1997.

[12] Robert Mahony et al. Complementary filter design on the special orthogonal group SO(3). *Proceedings of the 44th IEEE Conference on Decision and Control*, 2005.

[13] R.P.Kornfeld et al. Single antenna GPS based aircraft attitude determination. *J. Institute of Navigation*, 1998.

[14] B.Vik et.al. Nonlinear observer design for integration of DGPS and INS. *New Directions in Nonlinear Observer Design,ser. Lecture Notes in Control and Information Sciences*, 1999.

[15] FAA. Tso-c4c bank and pitch instruments. *Federal Aviation Administration*, 1959.

[16] FAA. Tso-c5e direction instrument, non-magnetic(gyroscopically stabilized). *Federal Aviation Administration*, 1989.

[17] Demoz Gebre-Egziabher. *Design and Analysis of Performance Analysis of a low-cost aided dead reckoning navigator.* Stanford University, 2004.

[18] J.Thienel and R.M.Sanner. A coupled nonlinear spacecraft attitude controller and observer with an unknown constant gyro bias and gyro noise. *IEEE Transactions on Automatic Control*, 2003.

[19] Jack B. Kuipers. *Quaternions and Rotation Sequences.* Princeton University Press, 1999.

[20] E.Glenn Lightsey and Jared Madsen. Three-axis attitude determination using global positioning system signal strength measurements. *J. Guidance, Control and Dynamics*, 2003.

[21] F. Landis Markley. Fast quaternion attitude estimation from two vector measurements. *J. Guidance, Control and Dynamics*, 2002.

[22] M.Greene and V.Trent. Software algorithms in air data attitude heading reference systems. *Aircraft Engineering and Aerospace Technology*, 2003.

[23] Kevin M.Passino and Stephen Yurkovich. *Fuzzy Control*. Addison Wesley, 1998.

[24] Malcolm D. Shuster. A Survey of Attitude Representations. *Journal of Astronautical Sciences*, 1993.

[25] S.Salcudean. A globally convergent angular velocity observer for rigid body motion. *IEEE Transactions on Automatic Control*, 1991.

[26] Nikolas Trawny and Stergios I.Roumeliotis. Indirect Kalman Filter for 3D attitude estimation. *A Tutorial for Quaternion Algebra*, 2005.

[27] Grace Wahba. A least-squares estimate of spacecraft attitude. *SIAM Review*, 1965.

Appendix A

Kalman Filter Formulation

A.1 Overview

The development of an extended Kalman filter for quaternion attitude estimation is addressed in the following sections. The Kalman filter is used to estimate errors in the attitude quaternion and gyro bias. The development of a state-space model for the Kalman filter is based on [26].

A.2 Extended Kalman Filter

The following data inputs are used in the Kalman filter algorithm:

- Triad of gyroscopic rates
- Triad of accelerations
- Triad of magnetic measures
- True airspeed computed by an air data system

Using true airspeed as an aiding input allows compensation for linear accelerations in determining the reference attitude quaternion. The state-space model for the filter can be written by starting with the gyro measurement model, assuming that the deterministic errors have been calibrated. If the deterministic errors in gyros are assumed to be calibrated, the gyro model can be written as

$$\omega_m = \omega_T + b + \eta_r \tag{A.1}$$

where ω_m and ω_T are the measured and the true angular rates, b is the bias and η_r is the rate noise and assumed to be white. If the estimated rate is $\hat{\omega}$, then

$$\hat{\omega} = \omega_m - \hat{b} \tag{A.2}$$

$$\omega = \hat{\omega} - \delta b - \eta_r \tag{A.3}$$

where $\hat{b}$ is the estimated bias and δb is the bias error. If the estimated attitude quaternion is represented by $\hat{q}$ and the true attitude quaternion by q, then the quaternion error can be represented as the incremental rotation δq necessary to rotate the estimated quaternion to align with the true quaternion.

$$q = \delta q \otimes \hat{q} \tag{A.4}$$

The true and estimated attitude quaternion dynamics are given by the equations

$$\dot{q} = \frac{1}{2}\begin{bmatrix} 0 \\ \omega \end{bmatrix} \otimes q \tag{A.5}$$

$$\dot{\hat{q}} = \frac{1}{2}\begin{bmatrix} 0 \\ \hat{\omega} \end{bmatrix} \otimes \hat{q} \tag{A.6}$$

The quaternion error dynamics can be derived from the above equations as

$$\dot{\delta q} = -\Theta(\hat{\omega})\delta q - \frac{1}{2}\delta b - \frac{1}{2}n_r \tag{A.7}$$

The bias error dynamics are modeled as a first order Gauss Markov process as

$$\dot{\delta b} = -\beta \delta b + n_w \tag{A.8}$$

where n_w is the driving noise process of the Gauss Markov process and $\Theta(\hat{\omega})$ is the skew-symmetric matrix

$$\Theta(\hat{\omega}) = \begin{bmatrix} 0 & -\omega_z & \omega_y \\ \omega_z & 0 & -\omega_x \\ -\omega_y & \omega_x & 0 \end{bmatrix} \tag{A.9}$$

The continuous-time state and measurement equations for the quaternion and bias errors is given by

$$\begin{bmatrix} \dot{\delta q} \\ \dot{\delta b} \end{bmatrix} = \begin{bmatrix} -S(\hat{\omega}) & -\frac{1}{2}I_{3x3} \\ 0_{3x3} & -\beta I_{3x3} \end{bmatrix} \begin{bmatrix} \delta q \\ \delta b \end{bmatrix} + \begin{bmatrix} -\frac{1}{2}I_{3x3} & 0 \\ 0 & I_{3x3} \end{bmatrix} \begin{bmatrix} n_r \\ n_w \end{bmatrix} \tag{A.10}$$

$$z = \begin{bmatrix} I_{3x3} & 0_{3x3} \end{bmatrix} \begin{bmatrix} \delta q \\ \delta b \end{bmatrix} + \begin{bmatrix} v_1 \\ v_2 \\ v_3 \end{bmatrix} \tag{A.11}$$

In formulating the above equations, the attitude errors are assumed to be small and only the vector components of the quaternion are considered. The process noise covariance and the measurement noise covariance matrices are given by

$$Q = \begin{bmatrix} \sigma_g^2 I_{3x3} & 0_{3x3} \\ 0_{3x3} & \sigma_{gm}^2 I_{3x3} \end{bmatrix} \tag{A.12}$$

$$R = \sigma_a^2 I_{3x3} \tag{A.13}$$

where σ_g^2 is the rate noise covariance, σ_{gm}^2 is the covariance of the Gauss Markov process modeled using experimental autocorrelation, and σ_a^2 is the measurement noise covariance. The discretized versions of the matrices are given by [7]:

$$A = exp(F\Delta t) \tag{A.14}$$

$$Q_d = GQG^T \tag{A.15}$$

$$R_d = \frac{R}{\Delta t} \tag{A.16}$$

where F is the system matrix in the state equation. The computation of the state transition matrix A is performed by using a Taylor's series approximation for the exponential, following the treatment in [8]. The difficulty in accurately calculating the noise variances, especially for gyro bias drift modeled as an exponentially correlated process, introduces errors in the initialization values for the covariance matrices Q and R. As a result, optimality of the Kalman filter is difficult to achieve in practice. Therefore, the error covariance P_k at each step is updated using the generalized update equation that holds for any Kalman gain - optimal or otherwise [7]:

$$P_k = (I - K_k H_k) P_k{}^{-} (I - K_k H_k)^T + K_k R_k K_k^T \tag{A.17}$$

The reference attitude quaternion is derived from acceleration and magnetometer measurements, along with the true air speed. Since the y-axis accelerometer does not provide any information about the roll attitude during a non-slipping turn, true airspeed and inertial yaw rate are used to derive the reference roll attitude using the equation:

$$tan(\phi) = \frac{U\dot{\Psi}}{G} \tag{A.18}$$

where U is the true air speed in meters per second, $\dot{\Psi}$ is the Euler yaw rate in rad/sec in the local reference frame and G is the acceleration due to gravity. The measurement input for the Kalman filter is the quaternion error between the reference and the quaternion updated using the current body rates and bias estimates.